



IN THE UNITED STATES PATENT AND TRADEMARK OFFICE

In re Application of:

Reinhard Janka

Serial No.: 10/009,287

Filed: November 6, 2001

Art Unit: 1743

Confirmation No.: 5952

Examiner: Yelena G. Gakh

Atty. Docket No.: 500343.20141

METHOD AND SYSTEM FOR
DETECTING THE LIGHT COMING
FROM A SAMPLE

DECLARATION OF DR. KLAUS WEISSHART

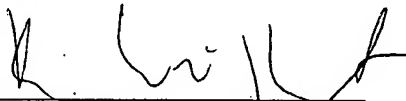
I, Klaus Weisshart, do hereby declare that:

1. I am currently Product Manager of the Microscope Division at Carl Zeiss Jena GmbH.
2. In 2004, I co-authored the article *The LSM 510 META – ConfoCor 2 System: An Integrated Imaging and Spectroscopic Platform for Single-Molecule Detection* by Weisshart et al. (Current Pharmaceutical Biotechnology, Vol. 5, No. 2, 2004) (the “article”), attached hereto as Exhibit “A.”
3. The first paragraph of the article states: “The demand for measuring correlation functions within a cellular environment was met by Carl Zeiss in the year 2000 by combining ConfoCor 2 and LSM (laser scanning microscope) detection modules in one integrated platform.” (*Id.* at 1.)
4. Carl Zeiss did combine ConfoCor 2 and LSM detection modules in one integrated platform (the “platform”).
5. The platform was not in public use or on sale in the United States, however, until May 23, 2000.

6. Specifically, on May 23, 2000, Carl Zeiss, Inc., a subsidiary of Carl Zeiss Jena GmbH, sold the platform to Boehringer Ingelheim Research and Development, whose offices are located at 175 Briar Ridge Road, Ridgefield, Connecticut 06877, U.S.A. On May 26, 2000, Carl Zeiss, Inc. purchased the platform from Carl Zeiss Jena GmbH. Then, on August 10, 2000, Carl Zeiss Jena GmbH generated invoice number 2040118607 for delivery of the platform to Carl Zeiss, Inc. (See Invoice dated 8/10/00, attached hereto as Exhibit "B.")
7. Approximately three months earlier, on February 22, 2000, Applicants filed German application 100 08 594.6, an application to which U.S. Application No. 10/009,287 claims priority.
8. Thus, German application 100 08 594.6 was filed before the platform was on sale or in public use in the United States.

I further declare that all statements made herein of my own knowledge are true and that all statements made on information and belief are believed to be true, and further that these statements are made with the knowledge that willful false statements and the like so made are punishable by fine or imprisonment, or both, under Section 1001 of Title 18 of the United States Code and that such willful false statements may jeopardize the validity of the application and any registration resulting therefrom.

Date: 06.11.07


Klaus Weisshart

The LSM 510 META - ConfoCor 2 System: An Integrated Imaging and Spectroscopic Platform for Single-Molecule Detection

Klaus Weisshart^{1,*}, Volker Jüngel¹ and Stephen J. Briddon²

¹Carl Zeiss Jena GmbH, Carl-Zeiss-Promenade 10, 07745 Jena, Germany and ²Institute for Cell Signalling, University of Nottingham, Nottingham NG7 2UH, United Kingdom

Abstract: Fluorescence Correlation Spectroscopy (FCS) has developed into a routine method to quantitatively study diffusion of molecules and kinetic processes. FCS has recently become popular to complement live cell imaging with biophysical information. The enabling technology has been commercially realised by combining laser scanning microscopes and fluorescence correlation spectrometers in one integrated platform. This article provides an overview of the Zeiss solution of such a combined instrument, the LSM 510 META / ConfoCor 2 system. We focus on the instrumental set up as well as technical advances and improvements in the software that controls FCS data acquisition and evaluation. In addition, we outline the calibration of the instrument and the work flow for data analysis with emphasis on *in vivo* pharmacological applications.

INTRODUCTION

The initial impetus for Carl Zeiss to develop a commercial system for fluorescence correlation spectroscopy (FCS) stemmed from Manfred Eigen and Rudolf Rigler in 1993. In cooperation with EVOTEC Biosystems, Hamburg, Carl Zeiss developed its first fluorescence correlation spectroscope, subsequently released in 1995 under the trademark ConfoCor. The system was designed to perform auto-correlation measurements for studying molecular interactions in solution. The first CZ workshop with the new system was organised by Rudolf Rigler in October 1995 at the Karolinska Institutet, Stockholm. Numerous workshops followed in the succeeding years and this tradition has continued to the present. 1997 saw the development of a first ConfoCor prototype, called ConfoCor 2, based on a two-channel detection system for measuring cross-correlation. Prior to its release in 1999, the system's performance was evaluated in the laboratories of Manfred Eigen and Rudolf Rigler. The major features of the instrument are based on these scientists' experiences and suggestions and have been reviewed previously [1]. The demand for measuring correlation functions within a cellular environment was met by Carl Zeiss in the year 2000 by combining ConfoCor 2 and LSM (laser scanning microscope) detection modules in one integrated platform. This unique combination set the stage for studying dynamic processes in the cell with an unprecedented sensitivity. This system will be discussed here with reference to the status of the current version, release 3.2. We will mainly focus on the ConfoCor 2 features, the unit used for single-molecule detection, and discuss only those features of the LSM 510 that are needed and useful in combination with ConfoCor 2 in cellular studies. Finally, the last section focuses on potential applications for the ConfoCor 2 in pharmacological studies.

INSTRUMENTAL SET-UP

A schematic drawing of the ConfoCor 2 - LSM 510 instrument is shown in Fig. (1). It consists of the following modules [1]: the FCS and LSM detection units, both of which are directly coupled to the Axiovert 200 microscope stand; the laser unit; the avalanche photodiode (APD) detection box; the electronic controls unit and a PC for data processing. Such a modular design gives the user the flexibility to work with solutions or in a cellular environment, and provides for specific interfaces such as the fibre coupling devices for laser illumination and detection, or the software for data transfer and handling. Both detection units feature folded beam paths for compactness and stability. All mechanically moving parts as well as the light attenuation are controlled by computer software. Control of both detection units is managed by the same software package employing, in part, the same laser units and electronics. Switching between the different modes proceeds automatically by directing the light via mirrors into the respective detection head. An existing mono unit can easily be upgraded to a combination system. The combination of both detection units is of considerable advantage in studying molecular interactions and diffusion processes in cells.

The Microscope Stand

The Axiovert 200 M is the motorized version of the CZ high-end inverted microscope. It serves as a base for the ConfoCor 2 and ConfoCor 2 - LSM 510 combination. It has two identical optical ports (side and base-port) that allow for the simultaneous attachment of both an LSM and FCS detection unit at either site. The Axiovert 200 M can be used without restrictions, thus epifluorescence with an HBO lamp or transmitted light provided by a HAL lamp can be used without compromise. As an option for the transmitted light path it is possible to couple an additional light source into the microscope. This allows the user to achieve other optical set

*Address correspondence to this author at the Carl Zeiss Jena GmbH, Carl-Zeiss-Promenade 10, 07745 Jena, Germany; E-mail: weisshart@zeiss.de

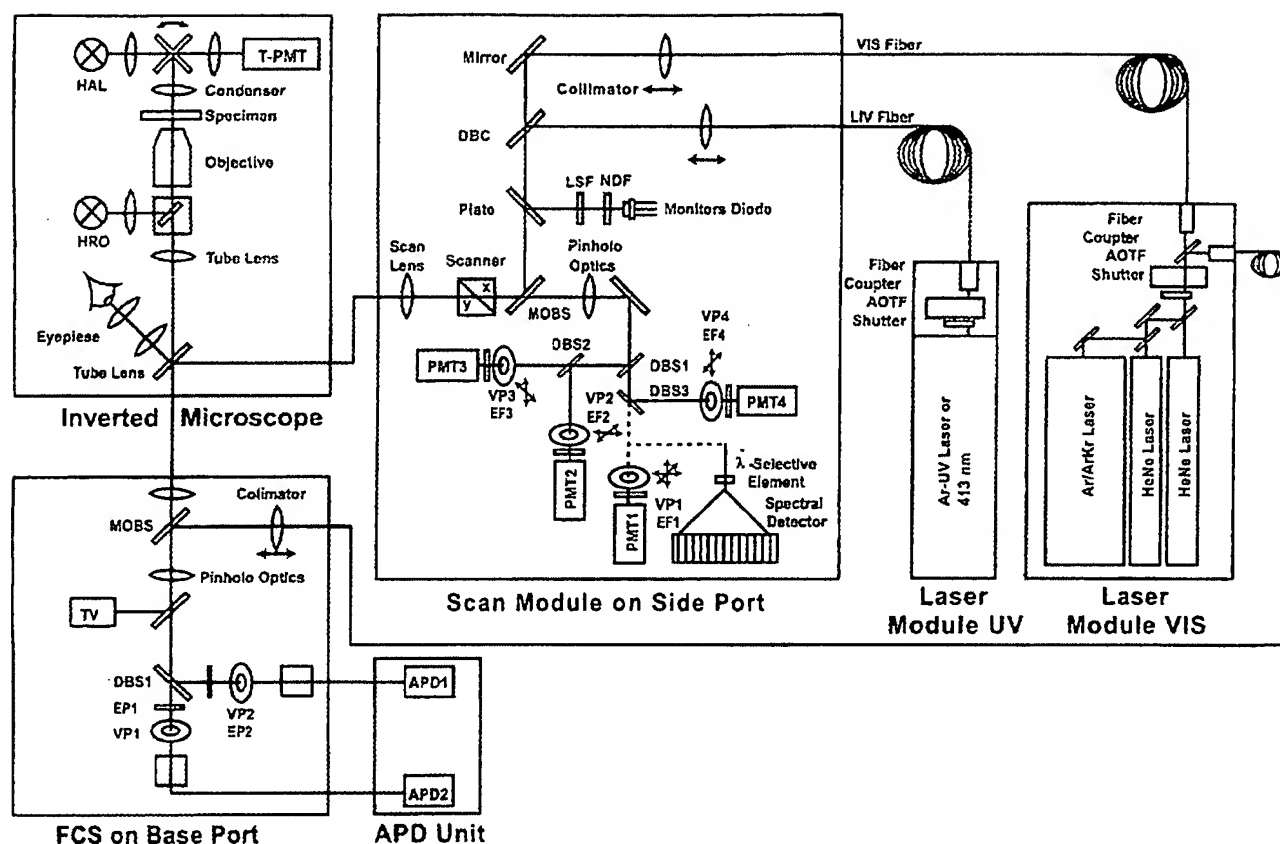


Fig. (1). Schematic set up of ConfoCor 2 -- LSM 510 system.

ups, for example TIRF illumination [2] or the production of two foci [3]. The C-Apochromat 40x, N.A. 1.2 water immersion lens is highly recommended as the objective due to its excellent chromatic aberration correction between wavelengths from 400 nm to 650 nm. Whereas the position of the laser beam is controlled by scanning mirrors in the LSM head, a scanning stage is used for this purpose in the FCS module. The scanning stage (max. movement range 120 mm x 100 mm, speed up to 10 mm/s) has a positional accuracy of about 1 μ m. If more accuracy is required, a piezo stage can be conveniently mounted onto the scanning stage. The piezo stage has a motion of 100 μ m x 100 μ m with a precision of 10 nm in a closed loop operation. The scanning stage permits analysis of a selected area in x, y or x-y planes to pinpoint a structure of interest (Fig. (2)). The highest precision can be obtained using the piezo stage. In addition, z-scans are also possible with the motorized nose-piece with step sizes of 50 nm. During the scan procedure the laser power can be lowered substantially to avoid bleaching of the sample. The pixel dwelling time during scanning amounts to 50 ms, the movement from pixel to pixel approximately 200 ms for the piezo stage.

The Laser Modules

The laser unit for visual light is shared between the FCS and LSM detection modules. A mirror conveniently switches

between the fibres that couple to either of the modules. The laser module is equipped with two fibre ports, but can be extended for a third one. Coupling of the laser lines into the scanning heads is performed via polarisation-retaining monomode fibres. The light is polarised vertically with respect to the major beam splitter. For flexible excitation, the VIS laser unit combines three different lasers: an argon ion laser with emission lines of 458, 488 and 514 nm and two HeNe lasers adding 543 nm and 633 nm excitation laser lines. Each laser line passes through an acousto-optical filter (AOTF) that is used to select and attenuate each individual line through the interaction of light with the travelling acoustic wave within an anisotropic crystal medium [4]. A second laser source such as a laser diode, UV laser or NLO laser can also be added for the LSM head. In the case of FCS it is possible to select as many as two wavelengths for a simultaneous excitation of the sample. Their intensities can be adjusted independently of each other with the AOTF by an attenuation factor of up to 10^6 . With the LSM, attenuation is up to 10^3 -fold with 4 lasers in use at a time. The higher attenuation capability with the FCS is needed due to the 1000-fold higher sensitivity of FCS compared to imaging. Shutters and line filters in front of the HeNe lasers and Argon laser, respectively, can be optionally operated to efficiently block out any laser line not in use in auto-correlation experiments.

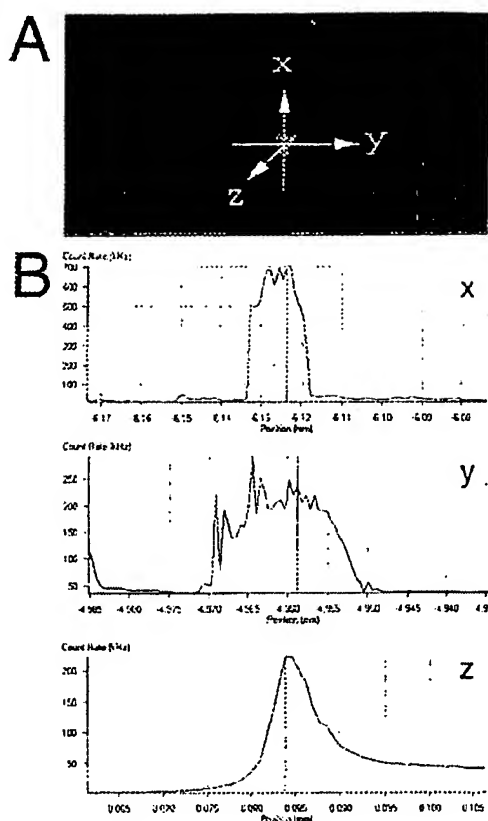


Fig. (2). X-, Y- and Z-Scan (panel B) through a PML-body (panel A) and positioning the beam in x, y and z (specimen kindly provided by L. Schmiedeborg and P. Hemmerich, IMB Jena).

The PC

A PC in the upper performance class is used to control the ConfoCor 2 - LSM 510 system and to acquire/evaluate data. Data exchange between the electronic module and the PC is achieved via an ultra-wide SCSI interface. In release 3.2 the software is run with the 32-bit Windows 2000 operating system. It can control the hardware and conveniently evaluate images and measured data. Both single measurements and software-controlled multiple measurements are possible. The software permits measuring techniques to be defined for later use in software-controlled automatic measuring processes. With respect to the FCS, auto-correlation and cross-correlation functions are calculated from the raw data quasi-simultaneously with the actual measurements. Furthermore, the primary data can be stored to allow individual evaluation by the user. To evaluate correlation curves, a software module is available to match the measured data to model functions using a non-linear fitting technique.

Detection Units

The FCS and LSM detection units combine the major components for laser light illumination and fluorescence light detection (see Fig. (1)). In both cases light from any laser source is passed through a collimator producing a parallel beam that, by using a major beam splitter (MDBS),

is reflected and focused via the objective into the sample. The C-Apochromat 40x / NA 1.2 water-corrected objective features an excellent working distance of about 0.14 - 0.18 mm into the sample and the high detection efficiency needed for FCS experiments. It produces a diffraction-limited spot in the volume range of 0.25 femtolitre or less. The C-Apochromat 63x / NA 1.2 water objective can be used as an alternative, producing the same diffraction-limited spot. This is in contrast to the situation with the first generation ConfoCor, where the 40x objective produces an approximately two-fold bigger confocal volume, whereas volumes obtained with the 63x objective are comparable to the ConfoCor 2 results.

Fluorescence labelled molecules excited by the laser beam will in turn emit photons of a longer wavelength. This light is collected by the same objective (epifluorescence illumination) and, in contrast to the reflected excitation light, will pass the major beam splitter. The emitted light is then directed through the pinhole optics, an array of highly corrected lenses that project light from the focal plane onto a pinhole (VP), which is placed in a conjugated focal plane. Thus, only light from the focal spot is passed efficiently and directed to the detectors, whereas all background signals originating from non-focal areas are sufficiently suppressed. Secondary beam splitters (DBS) (1 in the ConfoCor 2; up to 3 in the LSM 510) behind the pinhole optics can divide the emitted light into 2 or up to 4 channels, respectively, each possessing their own pinhole. Thus, in case of the ConfoCor 2 the secondary beam splitter is used for further spectral separation in cross-correlation measurements. To direct the light to one of the two available channels in auto-correlation experiments, a plate or a mirror is used for channel 1 or 2, respectively. Before reaching the detector, the light passes through emission filters (EF). These are placed in front of, or behind the pinholes in the LSM 510 and ConfoCor 2, respectively. These filters are designed to define the band-width of the detected light and suppress any residual reflected excitation light or diminish light originating from cross-talk. Both the beam splitters and the emission filters have to be selected depending on the excitation and emission spectrums of the dyes in use. It follows that a variety of filters are needed for performing FCS experiments. All filters inside both detection units are mounted on motorised wheels that hold up to eight filter positions (Table 1). It should be noted that filters are easily exchanged on site for the secondary beam splitters and the emission filters. However, changing filters in the major beam splitter require adjustments that can only be conducted in the factory.

The detected light is finally directed directly to photomultiplier tubes (PMT) in the LSM 510, or enters a fibre that guides the light to the avalanche photodiode (APD) detector of the ConfoCor 2. With respect to the optical beam paths in the ConfoCor 2 the total amplification is given by $M_{tot} = 10/3 M_{ob}$, where M_{ob} is the magnification of the objective. Therefore, a voxel 1 μ m in each dimension would be transformed into a rugby ball shape with x and y each having dimensions of 0.132 mm, while z is 17.4 mm (see Fig. 3). We want to point out that in the LSM 510, channel 3 can be equipped with a fibre out instead of a PMT, giving the user

Table 1. Standard Beam Splitters and Filters in the ConfoCor 2 Rel 3.2 Detection Head

Main beam splitter	Secondary beam splitter	Emission filter 1	Emission filter 2
HFT 458	NFT 500	BP 530-600	BP 475-525
HFT 488	NFT 570	BP 560-615	LP 475
HFT 514	NFT 610	LP 560	BP 505-530
HFT 543	NFT 635	LP 585-615	BP 505-530
HFT 633	NT 50/50	LP 585	LP 505
HFT 458/543	Plate	LP 600-650	BP 530-600
HFT 488/543	Mirror	LP 650	LP 530
HFT 488/633		Change position	BP 600-650

Abbr. HFT = main beam splitter; NFT = secondary beam splitter; EF = emission filter; LP = long pass, BP = band pass.

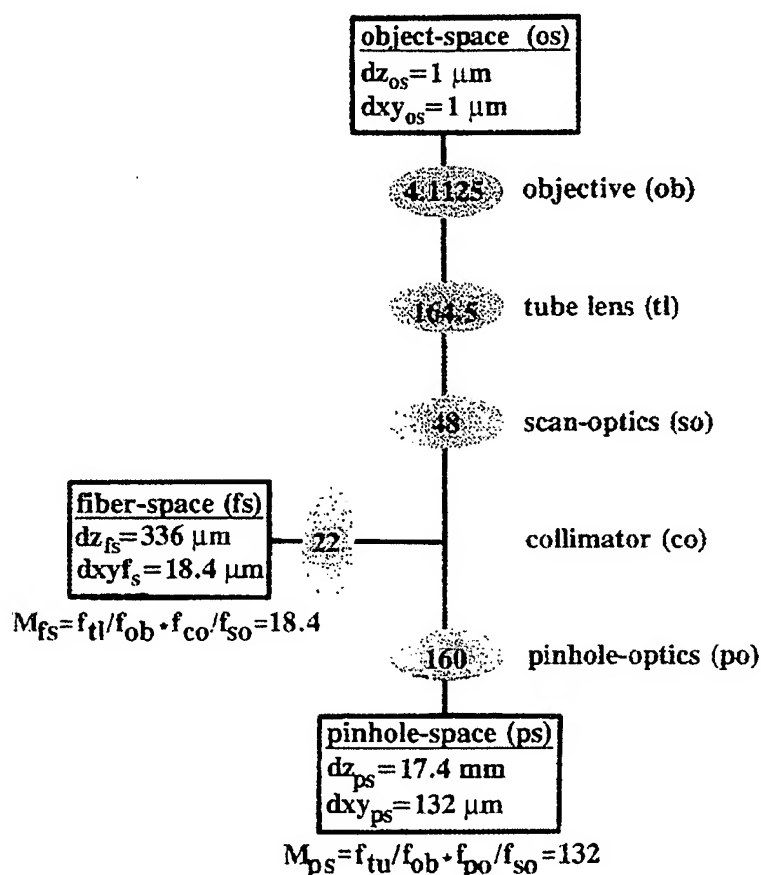


Fig. (3). Transformation of a $1 \mu m$ displacement ($dxyz$) in the sample space into the fibre and pinhole spaces in the ConfoCor 2. Numbers in the lens' symbols represent focal lengths (f) in nm. The calculation of magnification (M) is indicated. The magnification in the pinhole space corresponds to M_{tot} .

the option of directing the emitted light to other detection units. In addition, in channel 1 the single PMT can be replaced by the META detector, an array of 32 PMTs. In this case the emitted light is split into its spectral components via a diffraction grating located after the pinhole and is then

projected to the PMT array. It is therefore possible to obtain a spectral signature of the sample and via linear unmixing algorithms and known spectral signatures of the dyes, this can be used to distinguish true signal contributions from cross-talk, a procedure called emission fingerprinting [5, 6].

All pinholes are controlled by the software in x,y planes in the LSM 510. In addition, the pinhole in channel 1 can also be adjusted in the z plane. In the ConfoCor 2 both motorised pinholes can be controlled separately in xyz planes for optimal count rate adjustment with a precision of about 2 μm . The use of two pinholes has the advantage that both of them can be positioned individually to their optimum location for both colours, eliminating residual non-ideal aspects of the optical components. This distinguishes the ConfoCor 2 from other prototypes for cross-correlation based on ConfoCor [7]. In addition, the diameter of the pinholes can be varied between 10 μm and 200 μm . However, the useful upper limit in the case of the ConfoCor 2 is set by the diameter of the fibre coupling to the APDs, which is approximately 130 μm . The pinhole coordinates and the collimator position are stored for each beam path created, and are recalled when starting a method using this beam path. Therefore, pinhole and collimator adjustments do not need to be repeated each time a new method is called up. It should be emphasised that in the ConfoCor 2 the pinholes are not placed in the image plane of the tube lens. Using additional optical components a smaller cross section of the beam is formed in the detection unit. This facilitated a compact design that makes the instrument less sensitive to environmental influences such as vibrations and temperature shifts. In fact, once set, the pinhole position is stable over weeks. The smaller cross section also permits the use of smaller filters that are more optically flat and hence exhibit a higher quality optical wavefront.

For dual colour cross-correlation experiments the major beam splitter has to reflect two laser lines used for excitation and transmit two different spectral bands from the emission site. It is essential that all optical components are of high quality for cross-correlation to be detected efficiently. As a general rule to reduce cross-talk as much as possible, dyes should be chosen that have well separated excitation and emission spectra. Special filters for the use of wavelengths 458/543, 488/543 and 488/633 have been incorporated into the basic filter set (Table 1). The position of pinholes for channels 1 and 2 are optimised for emission wavelengths longer than 560 nm and shorter than 650 nm, respectively.

Especially designed for positioning the confocal volume in solution, the laser beam can be directed via a mirror onto a CCD detector chip (TV) in the ConfoCor 2 head. This allows detection of the glass surface by a reflected light spot and hence the assurance, by simply focussing up, that the confocal volume element is in the sample. For cell measurements, the LSM is used for selecting the position. In this case a ConfoCor 2 measuring point is simply marked in an LSM image. After switching to FCS operation, FCS measurements will be conducted at the selected site.

The APD Detection Box

The fluorescent light is coupled directly after the pinhole to multimode fibres, therefore the detectors can be placed outside the ConfoCor 2 detection unit. This has the advantage that the detection head can be kept compact, since an APD is large compared to a PMT, and it also avoids heating of the optical components. Connection of the fibre out to the

detector is via FC fibre connectors, meaning instruments other than APDs can be connected. The APDs presently used in the ConfoCor 2 are of the type SPCM-AQR-13-FC (Perkin Elmer). They show a low background signal (dark count rate < 250 Hz) and are essentially devoid of after pulsing problems. The pulse length of the detector is approximately 25 ns and its dead time 35 ns. The electronics extend the dead time to 50 ns, which results in a time resolution for counted photons of 20 MHz. The detection efficiency of the APDs strictly depends on the wavelength. The maximum sensitivity of 65% is obtained around 650 nm compared to 45% at 500 nm. This necessarily affects the spectral sensitivity of the detection channels, channel 1 being more sensitive than channel 2 [1]. Hence, a seemingly small cross-talk contribution from the blue dye into the red channel can be significant and should be corrected for, if cross-talk exceeds 10% of the signal. The detected incoming photons are converted to TTL pulses, which in turn are transferred to the electronic control unit.

The Electronic Control Unit

The electronic module combines the major components of data recording, of AOTF control and of the DSP (digital signal processor), as well as the trigger interface. For LSM510 - ConfoCor 2 combi operation, the LSM 510 electronic module can be easily upgraded into a LSM 510 - ConfoCor 2 combi electronic module.

In the control unit, the first analysis step takes place during an FCS experiment. Time intervals between the incoming TTL pulses are recorded in discrete units and transmitted via a fast SCSI connection to the computer. The normalised correlation function is then calculated via a specially developed software correlator and the curve displayed in real time. This means that within duration of the measurement, the correlation function is constantly recalculated. Three correlation functions can be computed simultaneously: the two auto-correlation functions of each detection channel and a cross-correlation function between them. The raw data, i.e. the arrival time of each photon, can be stored in binary format and used for post-acquisition data processing. These data can be reloaded and measuring times reselected for correlation analysis. This makes it possible to eliminate disturbing signals that would otherwise render the data set unusable (Fig. (4)).

The software correlator can process a few million photon detections per second in each channel. However, if the mean count rate exceeds 1.5 MHz a safety mechanism automatically switches off the APDs to avoid damage due to the high intensity. Additionally, a hardware temperature safety circuit will prevent overheating of the APDs. If raw data are stored on a PC during measurement, the mean count rate in both channels should not exceed 500 KHz, depending on the disk speed of the hardware being used.

FCS Data Processing

During measurement, the time between photons is recorded in a raw data file. The raw data are processed in quasi-real time and the following data sets are calculated

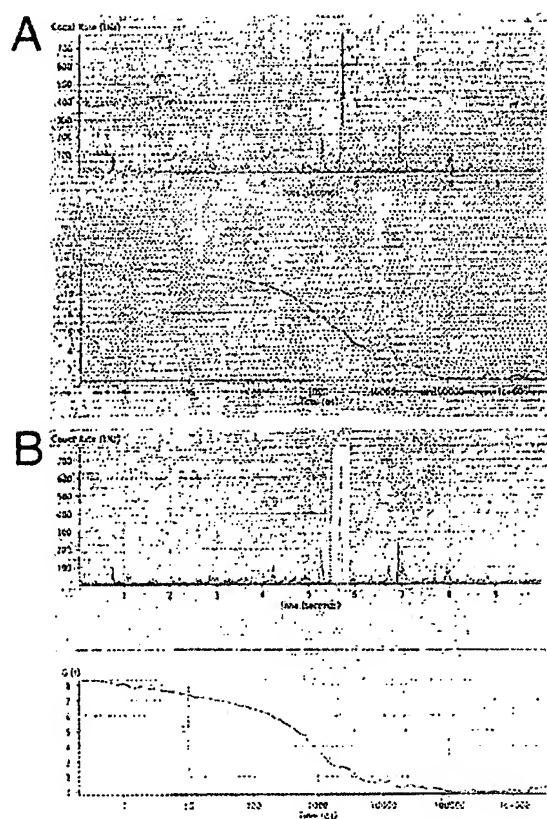


Fig. (4). Reanalysis of aggregation distorted data by the electronic dust filter. The cut-off region is indicated by a stippled box. Diffusion time decreased from the artificial 4 ms (panel A) to the expected 1 ms (panel B).

simultaneously: count rate trace, correlation (auto and cross), count rate histogram, coincidence histogram and pulse distance histogram (Table 2). As an option, the raw data can be stored and reloaded at later points in the ConfoCor 2 or other software programs.

Data Analysis

The count rate trace represents the averaged binned count rate versus measurement time, in other words photons / sec and therefore intensity. The bin window depends on the measurement time, whereby the bin window doubles, if 500 values are exceeded. In the first step, the binning time is 3.2 ms. For the next steps, the binning time (t_b) becomes $t_b = 3.2 \text{ ms} \times 2^n$. The measurement time (t_d), at which the binning time doubles is calculated according to $t_d = 3.2 \text{ ms} \times 500 \times 2^n$. In a cross-correlation experiment, the count rate traces of both channels are displayed. The trace can be used to identify bleaching or aggregation artefacts that can infringe on the correlation analysis, or be used to analyse the data by continuous photobleaching [8]. The data can be exported as ANSI or txt files for analysis using other programs and appropriate models (Table 3) [9-18]. The count rate trace is also used to indicate the time periods that are disregarded

in the correlation analysis if a dust filter is activated (see Fig. (4)).

To generate the photon count rate histogram, the number of pulses corresponding to detected photons is recorded versus their frequency. The binning time is 50 ns for the first 32 values in the first step. For the next steps the binning time doubles and this value is increased 16 times. Thus the binning time (t_b) at the end of step n can be calculated according to $t_b = 50 \text{ ns} \times 32 + 50 \text{ ns} \times 2^n \times 16$. If the raw data are available and reloaded, the user can define a constant binning time. For quantitative analysis, the data can be exported in ANSI or txt format.

In the pulse distance histogram, the time elapsed between two consecutive pulses is displayed according to their frequencies. The time distance starts with 50 ns, and is increased 32 times in the first step. For the next steps the time distance is doubled and increased linearly 16 times. The time distance (t_d) after step n is hence calculated as $t_d = 50 \text{ ns} \times 32 + 50 \text{ ns} \times 2^n \times 16$. The data have to be exported for quantitative analysis, which can be conveniently done in ANSI or txt format.

The coincidence histogram plots the frequency at which photons are recorded in channel 1 versus the frequency in channel 2. If photons occur simultaneously in both channels, all the data points should lie on a diagonal line. The two-dimensional histogram therefore gives a qualitative means for cross-correlating events. The data cannot be exported.

The correlation diagram shows the developing auto-correlation curve. In the case of a cross-correlation experiment, both auto-correlation and the calculated cross-correlation curves are displayed. The software allows the user to define which part of the curve should be displayed. Moreover, curves can be normalized for any correlation time and corrected for any offset from 1. The software provides for an on-line fit of the correlation data to a 3-D, free diffusion model. If the data should be made to fit another model (see Table 3 for common formulas for translational diffusion processes) then the data can be exported as ANSI or txt files, which allows them to be imported to any suitable fit program. Data in the .fcs format can also be imported directly.

The Raw Data Format

This data format is a true representation of the photon trace of both channels. The limits are dictated by the digitalisation of the data. Within this restriction, the data are therefore recorded without losses. The time between subsequent pulses is stored in units of elapsed clock cycles, i.e. the data are "run length encoded".

All data are recorded in 16 bit words (2 bytes). A word will be recorded on two occasions: either when a pulse is detected or the counter counting the elapsed clock cycles overruns 255 (FF in hex code). A single word contains the information on how many clock cycles (1 ... 255) have elapsed since the last word was recorded, in the first or low byte and in addition, what happened in the four cycles that are needed for data generation (bit1 ... bit4) in the second or

Table 2. Data Analysis. All Listed Data are Acquired Simultaneously

Name	Description	Acquisition	Calculation	Display	Analysis
Count rate	Photons / sec = intensity	1 or 2 channels	Binning	Intensity curve	Average intensity, bleaching
Auto-correlation	Analysis of interaction; one partner is labelled; differentiation by diffusion properties	1 or 2 channels	Multiple tau algorithm	Auto-correlation curve	Number of molecules; 2 diffusion times; 2 fractions; triplet time / fraction
Cross-correlation	Analysis of interaction; two partners labelled; differentiation by diffusion	2 channels	Multiple tau algorithm	Cross-correlation curve	Number of molecules; diffusion times
Coincidence histogram	Rare event detection Two partners are labelled	2 channels	Binning and counting	2-D count rate histogram	Separate software needed (use data export)
Count rate histogram	Analysis of interaction; one partner is labelled; differentiation by brightness	1 or 2 channels	Binning and counting	Count rate histogram	Separate software needed (use data export)
Pulse distance histogram	Time between photons	1 or 2 channels	Counting	Density curve	Separate software needed (use data export)
Raw data	Time between photons Stored as file using patented data compression	1 or 2 channels	Data compression	File name	Use data export for other software; reload for post acquisition data processing

high byte. This byte also contains information indicating in which channel a photon was recorded. The low byte is transferred first, then the high byte according to INTEL convention. The structure and an example of the recorded words are described in Tables 4 and 5. The first 30 bytes of a raw data file contain commentary information and should be neglected for data analysis.

The special proprietary format allows conservation of space at high count-rates and handling of dual channel data. The clock runs at a rate of 20 MHz. The minimum and maximum data transfer rates refer to the minimum and maximum clock rates that have passed before the counter overflow is activated. The maximum data rate transferred via SCSI is 10 Mbyte/s. In this case a pulse is registered in the 1st cycle. An additional 3 cycles are required for the overflow to transfer the data while not losing any data during this time, giving a total of 4 cycles. This results in $4 \times 50 \text{ ns} = 200 \text{ ns}$ to transfer the 2 bytes of information; hence a transfer rate of 10 Mbyte per 1 s. If no pulses are recorded the data transfer rate can drop to approximately 155 Kbyte/s. In this case the overflow starts at cycle 255. Including the 3 overflow cycles, there are $258 \text{ cycles} \times 50 \text{ ns} = 12\,900 \text{ ns}$ to transfer the 2 bytes.

The FCS Data Format

FCS data can be saved in binary and ANSI formats. The header in each case contains all the necessary information to identify a measurement with reference to how it was taken. The first data set represents the averaged count rate, the second the count rate histogram, the third the pulse density histogram and the last the correlation (with information on the dust filter). These four data sets are always treated as one block. For example, if two measurements have been taken these are treated in two blocks. In the case of cross-

correlation, the first three data sets build a block for one channel, followed by the block for the second channel. Then the auto-correlation and the cross-correlation functions are listed as a block.

The Correlator Software

In contrast to the ConfoCor that used the ALV500 board for hardware correlation, the ConfoCor 2 uses a software correlator. Both correlators use the so-called multiple tau algorithm that enables calculation of the correlation function over a wide range of lag or correlation times [15, 19, 20]. In this procedure, the time window in which the photon count rate is measured is enlarged with increasing sampling time, providing a logarithmic scale in the lag times. In contrast, a linear algorithm works with a constant time window, resulting in a smaller dynamic range in lag times. A disadvantage of the multiple tau method is that the data are averaged over a certain time window (correlation interval) and some parts of the information are lost.

The algorithm for auto-correlation functions is as follows (Fig. (5)): in the first correlation step all events within a certain correlation interval T are counted. In the ConfoCor 2, T in the first correlation step ($n=0$) equals 200 ns, which is 4 x the maximum sampling rate of 50 ns, as limited by the dead time of the APDs. This corresponds to a clock speed of 20 MHz. Thus, for this correlation interval a maximum of 4 events can be counted. These events/correlation intervals are shifted against themselves for a time interval τ . In the ConfoCor 2 software, the smallest τ equals $200 \text{ ns} = 0.2 \mu\text{s}$. τ is linearly increased by step sizes of 200 ns 16 times, i.e. the maximum correlation time in the first step is $16 \times 0.2 \mu\text{s} = 3.2 \mu\text{s}$. The direct and shifted events/correlation intervals are multiplied interval for interval and the products are added

Table 3. Model.

General expression for correlation function

$$G_{tot}(\tau) = 1 + d + B^2 \cdot A \cdot \prod_d G_d(\tau) \cdot \prod_k G_k(\tau) \cdot \prod_r G_r(\tau) \cdot \prod_a G_a(\tau)$$

d, offset from 1; B=1-I₀/I, background correction; I₀, background intensity; I, total intensity; A=G(0)-1=γ/N, amplitude; N, average number of molecules in the observation volume; γ, correction factor for PSF; ∏ G(τ) terms representing the contribution of diffusional (d), kinetic (k), rotational diffusion (r) and antibunching (a) processes

Expression for kinetic processes (k) including triplet state and blinking / flickering (exponential decay) and translational diffusion processes (d)

$$G_k(\tau) = \left(\frac{1 - T + T e^{-\frac{\tau}{\tau_T}}}{1 - T} \right) \text{ for reaction } B \xrightleftharpoons[k_r]{k_f} D : G_d(\tau) = \sum_{i=1}^m \Phi_i \cdot g_i(\tau) \text{ with } \Phi_i = \frac{f_i \cdot \eta_i^2}{\left(\sum_{i=1}^m [f_i \eta_i] \right)^2}$$

k_f & k_r, rates in forward and reverse direction; B & D, bright and dark states; τ_T=1/(k_f+k_r), relaxation time; T=k_r/(k_f+k_r), fraction of molecules undergoing conversion to dark state; Φ_i, fractional intensity for ith species; f_i=N_i/N, relative molecular fraction of ith species with the constraint Σ f_i=1; η_i, molecular brightness of ith species; g_i(τ), expression describing the diffusion characteristics

Free (f) and anomalous (a) 2D and 3D translational diffusion

$$g_{i,f2D}(\tau) = \frac{1}{\left(1 + \frac{\tau}{\tau_{D,i}}\right)} : g_{i,f3D}(\tau) = \frac{1}{\left(1 + \frac{\tau}{\tau_{D,i}}\right) \cdot \left(1 + \frac{\tau}{\tau_{D,i}} \cdot S^{-2}\right)^{1/2}} : g_{i,a2D}(\tau) = \frac{1}{\left(1 + \left[\frac{\tau}{\tau_{A,i}}\right]^{\alpha_i}\right)} : g_{i,a3D}(\tau) = \frac{1}{\left(1 + \left[\frac{\tau}{\tau_{A,i}}\right]^{\alpha_i}\right) \cdot \left(1 + \left[\frac{\tau}{\tau_{A,i}}\right]^{\alpha_i} \cdot S^{-2}\right)^{1/2}}$$

τ_D=r₀²/(4D), average residence time for free diffusion; D, diffusion coefficient; S=z₀/r₀, structural parameter; τ_A²=r₀²/H, average residence time for anomalous diffusion; α, temporal component; τ, transport coefficient of fractional dimension

Active transport or flow and combined flow with free 3-D translational diffusion

$$g_{i,fl}(\tau) = e^{-\left(\frac{\tau}{\tau_{F,i}}\right)^2} : g_{i,fl-3D}(\tau) = \frac{1}{\left(1 + \frac{\tau}{\tau_{D,i}}\right) \cdot \left(1 + \frac{\tau}{\tau_{D,i}} \cdot S^{-2}\right)^{1/2}} \cdot e^{-\frac{\left(\frac{\tau}{\tau_{F,i}}\right)^2}{1 + \frac{\tau}{\tau_{D,i}}}}$$

τ_F=r₀/v average residence time for flow; v, velocity

Table 4. Structure of Recorded Word

Byte	Bit	Information
LSB Low byte	0...7	Clock counter value (starting at 1) during the triggering event. Triggering events are pulse recordings or counter overruns. Zero is reserved and only transmitted at the end of the measurement.
MSB High byte	8	1 if a pulse is recorded in channel 1 during cycle bit1; otherwise 0
	9	1 if a pulse is recorded in channel 2 during cycle bit1; otherwise 0
	10	1 if a pulse is recorded in channel 1 during cycle bit2; otherwise 0
	11	1 if a pulse is recorded in channel 2 during cycle bit2; otherwise 0
	12	1 if a pulse is recorded in channel 1 during cycle bit3; otherwise 0
	13	1 if a pulse is recorded in channel 2 during cycle bit3; otherwise 0
	14	1 if a pulse is recorded in channel 1 during cycle bit4; otherwise 0
	15	1 if a pulse is recorded in channel 2 during cycle bit4; otherwise 0

Table 5. Example of a Recorded Word. The Table Shows Part of the Running Pulse Train (From Left to Right) Divided Into Clock Cycles. A "1" in the Corresponding Box Indicates that a Pulse Arrived in this Cycle at Channel 1 or 2. The "Counter" Row Shows the Counter Readings and the "Word" Row Indicates, When a Word is Recorded

Transmission				bt1	bt2	bt3	bt4							bt1	bt2	bt3	bt4		
Ch1				1		1						...							
Ch2					1							...							
Counter	120	121	122	123	0	0	0	1	2	3	4	...	254	255	0	0	0	1	2
Word							↑ W1										↑ W2		

The following word will be recorded:

At W1: high byte 00011001 (bit) = 19 (hex); low byte 123 (dec) = 7B (hex) \Rightarrow resulting word = 7B19 (hex)

At W2: high byte 00000000 (bit) = 00 (hex); low byte 255 (dec) = FF (hex) \Rightarrow resulting word = FF00 (hex)

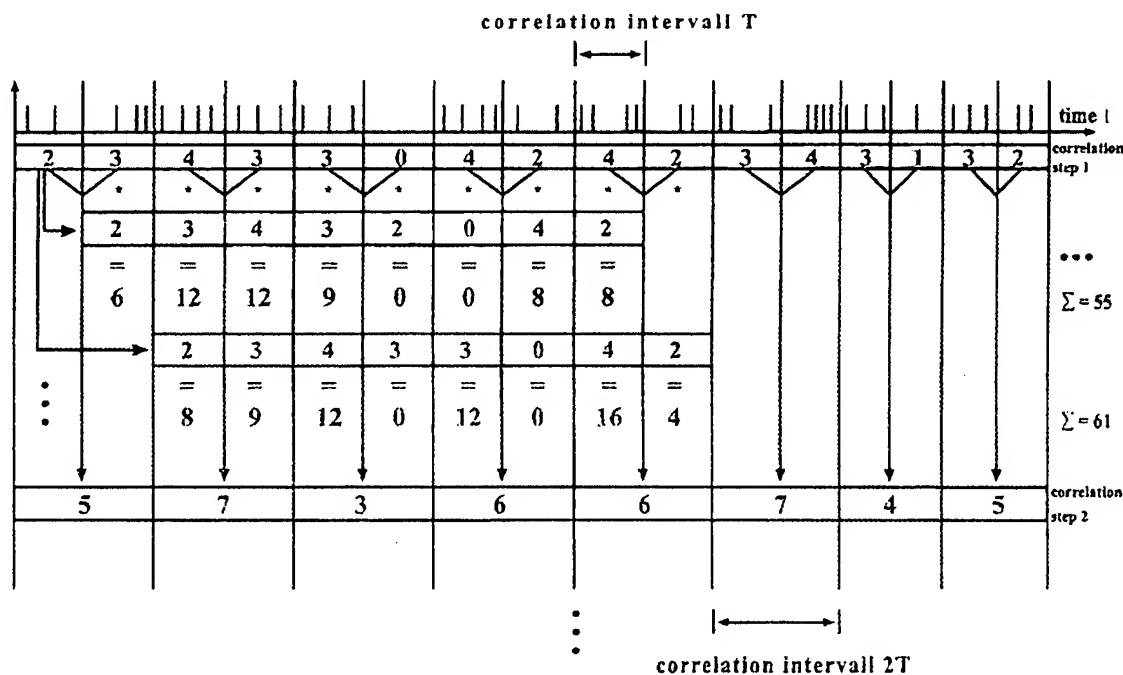


Fig. (5). Operational sequence of the multiple tau algorithm for auto-correlation.

together and normalised. The normalisation result is defined as: $(\text{result} \times \text{received clocks})/(\text{pulse}^2)$ for auto-correlation or $(\text{result} \times \text{received clocks})/(\text{pulseA} \times \text{pulseB})$ for cross-correlation. The received clocks counted equal 4 x the number of correlation intervals, which are defined by the measurement time. At the end the relevant data for the next correlation step are processed. Here, the correlation interval is increased by a factor of 2. Hence, the correlation interval (T) in the n -th correlation step is $T = 0.2 \mu\text{s} \times 2^n$. The initial lag time for a certain correlation step corresponds to the last lag time of the previous correlation step added to the respective correlation interval. This value is then linearly increased 8 times. Therefore after step n , the correlation or lag time (τ) ultimately corresponds to $\tau = 16 \times 0.20 \div 8 \times 0.2 \times 2^n \mu\text{s}$. The doubling of the correlation interval is performed

25 times. Thus the maximum is $\tau = 16 \times 0.2 + 8 \times 0.2 \times 2^{25} \mu\text{s}$.

With the cross-correlation algorithm, channel 1 is correlated against channel 2 (Fig. (6)). The correlator works in a manner similar to the one used for auto-correlation. In the first step, all events in each channel within a correlation interval T are counted. Then the direct events / correlation intervals of each channel are multiplied and the resulting products are summed and normalised. The events / correlation intervals in channel 2 are now displaced for the lag time τ . Subsequently, the direct events / correlation intervals of channel 1 are multiplied with the displaced events / correlation intervals of channel 2, interval for interval, and the products are summed and normalised. Finally, the data for the next correlation step are processed

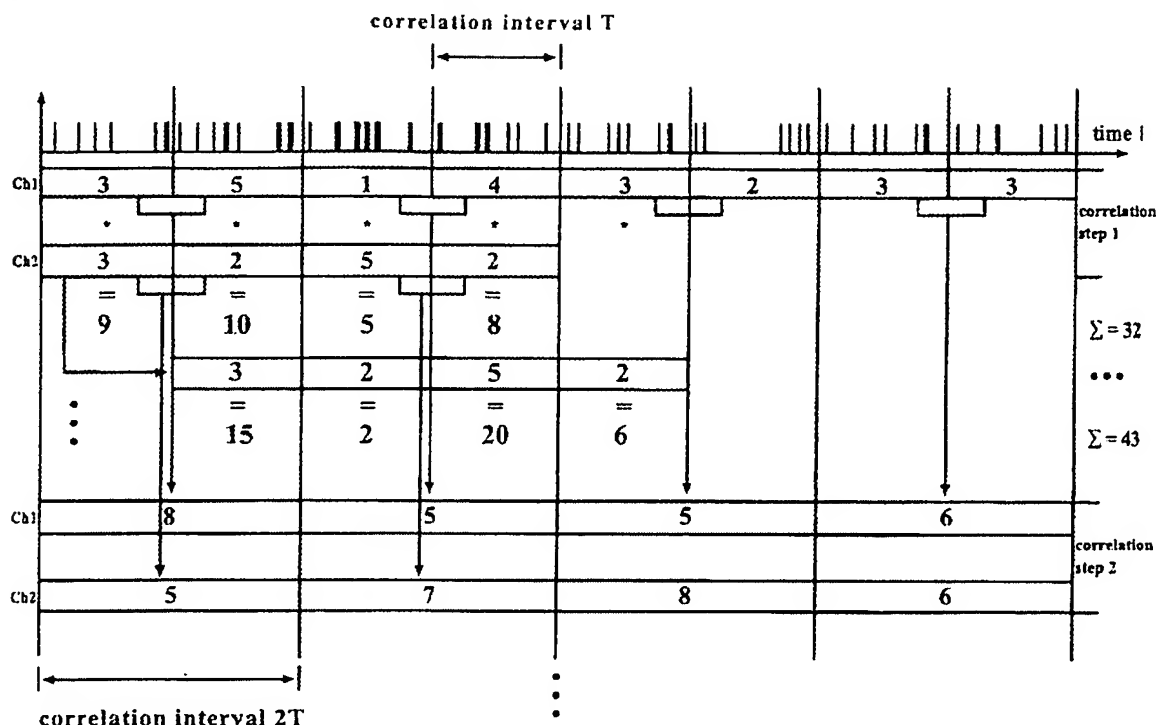


Fig. (6). Operational sequence of the multiple tau algorithm for cross-correlation

and the correlation interval is doubled. Correlation times are calculated as described above for auto-correlation.

Optical Considerations

The molecular detection efficiency (MDE) is strictly dependent on the excitation intensity profile $I(r, z)$ and the collection efficiency function $CEF(r, z)$:

$$MDE(r, z) = \epsilon \cdot I(r, z) \cdot CEF(r, z) \quad (1)$$

where the constant ϵ reflects the quantum yield of the fluorophore and the detector. The vector r denotes the position in the x, y plane and z the distance between this plane and the focal plane. The detection efficiency can be approximated by a three-dimensional Gaussian profile for a laser beam in a confocal detection set-up that under-fills the back aperture [19, 21]:

$$MDE(r, z) = \epsilon \cdot e^{-\frac{2r^2}{r_0^2}} \cdot e^{-\frac{2z^2}{z_0^2}} \quad (2)$$

where r_0 and z_0 denote the distances in radial and axial directions at which the intensity drops to $1/e^2$ of the maximum intensity I_0 . The calculation of the expected correlation function for one component without any photophysical process, based on these assumptions, leads to:

$$G(\tau) = \frac{1}{N} \left(\frac{1}{\left(1 + \frac{\tau}{\tau_{Di}}\right) \sqrt{1 + \tau^2 (S^{-2} \tau_{Di})}} \right) + 1 \quad (3)$$

where τ is the lag or correlation time, τ_D the average time a particle spends in the confocal volume, N the average

number of molecules in the confocal volume and $S = z_0/r_0$ the structural parameter.

In the ConfoCor 2, the back aperture (pupil diameter = 9.2 mm for the C-Apo 40x objective), is however overfilled by the $1/e^2$ of the collimated laser beam radius (diameter of 11 mm), producing a diffraction-limited spot in the sample [1]. Due to the large effective focussing angle the external Airy rings produced by the diffraction of light at the circular aperture of the objective are strongly reduced due to non-homogeneous illumination of this aperture. The smaller beam cross sections, in turn, mean smaller dichroic mirrors with higher optical quality can be used. Although the theory of Gaussian beams does not strictly apply to the ConfoCor 2 [21, 22], formula (2) is still in fact valid. This was proved using a scanning field optical microscope (SNOM 210, Carl Zeiss and Digital Instruments) to determine the excitation intensity profile with a spatial resolution of approximately 80 nm [1]. In addition, the truncated Gaussian intensity profile induces a slight broadening of the central spot and the $1/e^2$ radius r_0 of the focus hardly varies with z . The diameter of the pinhole (d_{PH}), which reduces the out of focus background, is usually set to 1 Airy unit: $d_{PH} = M_{tot} \frac{1.22\lambda}{NA}$.

Smaller pinhole diameters reduce the thickness of the optical slice, which results in a smaller structural parameter $S = z_0/r_0$.

The Fit Software

Fluctuations in the fluorescence signal recorded as photons can be described as deviations from the temporal average of the fluorescence signal:

$$\delta F(t) = F(t) - \langle F(t) \rangle \quad (4)$$

where the bracket indicates the time-averaged fluorescence signal. The mathematical function for the normalised auto-correlation function of intensity fluctuations is therefore, in the case where no bleaching occurs, given by:

$$G_{ij}(\tau) = 1 + \frac{\langle \delta F_i(t) \cdot \delta F_j(t + \tau) \rangle}{\langle F_i(t) \rangle \cdot \langle F_j(t) \rangle} = \frac{\langle F_i(t) \cdot F_j(t + \tau) \rangle}{\langle F_i(t) \rangle \cdot \langle F_j(t) \rangle} \quad (5);$$

$i=j$ for auto-correlation; $i \neq j$ for cross-correlation.

The fluorescence intensity is measured through the counted photons. To retrieve valuable information, the correlated data have to be fitted to an appropriate model. The mathematical model for the correlation function used in the fit module of the ConfoCor 2 is represented by:

$$G(\tau) = 1 + \frac{1}{N} \left(\frac{1 - T + T e^{-\tau/\tau_T}}{1 - T} \right) \left(\sum_{i=1}^n \frac{f_i}{(1 + \tau/\tau_{Di}) \sqrt{1 + \tau(S^{-2} \tau_{Di})}} \right) \quad (6)$$

Formula (6) is the intensity-normalised correlation function of fluorescence photons from translational diffusing particles under the assumption that the molecule detection efficiency is described by Gaussian profiles in radial and axial directions [4, 12]. n represents the fluorescent components that are subject to the normalisation constraint $\sum_{i=1}^n f_i = 1$, N the average number of fluorescent

molecules in the effective detection volume $V_{eff} = \pi^{3/2} r_0^2 z_0$, T and τ_T , respectively, the fractional population and decay time of the triplet state, f_i and τ_{Di} , respectively, the contribution and the translational diffusion time of the i -th fluorescent component and S is the structural parameter of

the instrumental set-up: $S = \frac{z_0}{r_0}$, where z_0 and r_0 are the

distances from the centre of the laser beam focus in the radial and axial directions, respectively, at which the collected fluorescence intensity has dropped by a factor of e^2 compared to its peak value for the Gaussian beam profile.

For many applications simpler modules than the one represented by (6) can be used: for example, models without triplet fractions ($T=0$) and different reductions to particular numbers of components (normally no more than 3). In the case of cross-correlation measurements, the triplet state model can be used as well. Thus, with a 50/50 plate, an auto-correlation measurement can be acquired simultaneously in both channels and also analysed by cross-correlation software. Artefacts due to electronic noise such as after-pulsing of the APDs can be detected by comparing the auto-correlation curves to the cross-correlation curve. In other cases, e.g. 2-dimensional diffusion or correction of an offset, the model can also be used by simply setting the structural parameter to high values (quasi-infinite) or fixing an additional component with an exceptionally high diffusion

time. However, in cells, there may also be more complicated models (see Table 3). In these cases, the user can export the correlated data to use them in other software programs.

The fit is based on the approximation of the experimental acquired correlation function to the theoretical function (6) with the normalisation constraint. The theoretical model is characterized by a final set of parameters (N , S , T , τ_T , f_1, \dots, f_n , $\tau_{D1}, \dots, \tau_{Dn}$). All parameters can be uniquely determined on the basis of only one measured correlation curve, provided that the number of components M is known. The parameters are derived by a Levenberg-Marquardt algorithm [23, 24]. The idea is to linearise the model (6) in a truncated Taylor series in order to make use of linear least-squares analysis and to obtain the desired minimum value of X^2 by an iterative sequence of calculations. Initial guesses are determined automatically based on the phase plane method [25, 26]. Thus, the path of data analysis is composed of a non-iterative phase used to generate the start values and an iterative procedure, starting the search with those initial values.

The algorithm does not produce reliable results in the case of a weak signal, the presence of different components of similar diffusion times, or considerable under-representation of one fraction (below 10%). Fitting results naturally becomes less accurate, the more parameters that have to be fitted. However, it is often possible to predetermine some of the parameters in preliminary experiments, the values of which can be fixed in the fitting routine. It also often helps to restrict the fit window, which can be carried out easily in the ConfoCor 2 fitting software.

The quality of the fit algorithm has been tested previously using simulations with defined model parameters [1]. If the signal to noise ratio of the correlation function was set to 20 for a 1 ms diffusion time, the deviation of the fit results was 1% for N , 4% for τ_D , 20% for the ratio of axes and even more for the triplet parameter. If the signal to noise value was set to 250, two fractions with their diffusion times differing by a factor of two could only be distinguished if their contribution was above 20%. However, a fraction of 10% could still be detected if the structural parameter was fixed. Of course, the greater the difference between diffusion times, the lower the % fraction that can be resolved. Likewise, in cross-correlation experiments the cross-correlated species has to contribute over 1% to the signal in order to be reliably detectable.

Correlation Analysis

The correlation signal increases with a smaller detection volume. Hence, the ConfoCor 2 has a better signal-to-noise ratio than the ConfoCor. Naturally, the diffusion time also decreases with a reduction in volume. For example, Rh6G shows a diffusion time of approximately 22 μ s with the ConfoCor 2 in contrast to 60 μ s, a typical value for the ConfoCor using the same 40x objective [1]. Biophysical processes, such as triplet states in the time range of 5 μ s or less, are independent of the confocal volume. In solution, the ConfoCor 2 gives exceedingly reproducible values. For examples we refer the reader to Jankowski and Janka [1]. With pure dyes, even the structural parameter, which is

normally difficult to derive from a fit, is quite stable: 5 – 5.5 for 488 nm and 8 – 8.5 for the 633 nm line. In auto-correlation experiments, molecules can be separated if their diffusion times are at least 1.6-fold apart, which requires a size difference of the molecules of 5-fold or more [27].

The signal-to-noise ratio (SNR) is proportional to the detection efficiency or the count rate per detected molecule η (cpm) and the square root of the measurement time T : $SNR \propto Q\sqrt{T}$ [28]. That means the higher the cpm, the less measurement time required for the same quality of data: for example, a two-fold higher cpm value would reduce the measurement time 4-fold. As a rule of thumb it is recommended to use a measurement time 1000-fold longer than the diffusion time of the molecule. The cpm depends on the quantum yield and other biophysical properties of the dye, as well as the sensitivity of the instrument, which depends in turn on the quality of the lenses and filters. The use of wider band passes can dramatically increase the cpm values. Also higher concentrations and laser powers can yield higher cpm values. For low concentrations and intensities, the noise due to the dark rate of the detectors significantly contributes to the signal. However, in both cases a maximum value can be observed and cpm values drop again when a threshold value is exceeded. For example, the 488 nm line set at a tube current of 6.1 A and an AOTF setting of 100% corresponds to approximately 1.5 mW at the back aperture of the objective. This causes the background signal to rise and results in lowered cpm values. If concentrations become too high, the fluctuations become less pronounced and this also leads to lower cpm values.

In the ConfoCor 2 η is not determined by the fit procedure. Instead, the correlation function between 2 to 10 μ s is averaged and considered to equal the inverse of the number of particles. The mean count rate divided by the number of particles then determines η . If the triplet state and triplet lifetimes do not exceed 30% and 5 μ s, they do not detract from the data by introducing errors. If particle numbers increase to high values, the correlation signal will be small. Optimum cpm values with most dyes are obtained at concentrations ranging from 10^{-7} to 10^{-8} M and laser intensities of 1 to 10%. However, one should keep in mind that these requirements are mostly not fulfilled in a cellular environment. First, laser powers have to be reduced as much as possible to avoid bleaching, and secondly, most systems used today are over-expressing systems. Nevertheless, the ConfoCor 2 has been successfully employed in auto-correlation studies using GFP-fusion or dye-labelled molecules [29, 30].

As pointed out earlier, if the diffusion times of two molecules are closer than 1.6-fold, the auto-correlation analysis according to (6) cannot distinguish between the two species. In this case the two components are then labelled with different dyes and their signals are spectrally separated into two channels, a procedure called dual colour cross-correlation [7, 31, 32]. Single labelled species (bound and unbound) are determined for each label by auto-correlation and double-labelled species are detected by cross-correlating

the signals of one channel with those of the other. If only one cross-correlated species is formed, formula (6) can be used if slightly modified. A true cross-correlated signal is distinguished by the absence of a triplet state, since it is very unlikely that the different labelled molecules will be in that state simultaneously. The occurrence of a triplet fraction is therefore due to cross-talk of the blue signal into the red channel. The cross-correlation amplitude is proportional to the number of double-labelled species and hence its meaning differs from those of the auto-correlation function:

$$G(0) - 1 = \frac{1}{N_{cr}} = \frac{N_{br}}{N_{acr} \cdot N_{abr}} = \frac{N_{br}}{(N_r + N_{br})(N_b + N_{br})} \quad (7)$$

N_r , N_b , N_{acr} , N_{nbc} , and N_{br} designate the number of the free red, free blue, total red, total blue and bound red-blue molecules, respectively. It is evident that the cross-correlated species contribute to both the numerator and the denominator, whereas the free molecules only contribute to the denominator. If not all partners are bound, the cross-correlation amplitude will always be smaller than the auto-correlation amplitudes due to formula (7). Nevertheless, if the contribution of the cross-correlated species is at least 1%, the reaction product can be detected with a good signal-to-noise ratio using the ConfoCor 2 [1, 33]. Recently, the ConfoCor 2 was successfully used to study the common transport of subunits A and B of cholera toxin by cross-correlation in living cells [34].

Using dual colours it is extremely important to overlap both confocal volumes as precisely as possible. The ConfoCor 2 possesses special correction optics that allow the localisation of each of the two confocal volumes to be adjusted relative to each other in x and y. The collimator setting can be used for maximum approach of the z position. Sizes of the confocal volumes can be partially adjusted by the pinhole diameter [33].

Cross-talk of the blue emission into the red channel reduces the signal quality and cannot be neglected if it exceeds 10%. Then the true number of cross-correlated particles has to be corrected for the cross-talk contribution:

$$G(0) - 1 = \frac{1}{N_{cr}} = \frac{N_b \cdot q + N_{br} \cdot (1 + q)}{(N_b + N_{br})(N_r + N_b \cdot q + N_{br} \cdot (1 + q))} \quad (8)$$

with $q = \frac{\eta_{rbb}}{\eta_{rrr}}$ being the fraction of correlated cross-talk and $\eta_{em,dye,ex}$ the molecular brightness values for the dyes at various excitation and emission wavelengths [11].

CALIBRATION OF THE INSTRUMENT

To obtain accurate parameters (diffusion coefficient and concentration of molecules) from correlation functions, it is essential to know the dimensions of the observation volume. The volume is characterized by the radial and axial beam waist r_0 and z_0 for which the laser intensity has dropped to e^{-2} of its maximum value. Although equipment is available to measure the volume element precisely, in normal circumstances such instruments are not available on an FCS set-up.

Instead, indirect methods can be employed using a sample with a defined diffusion coefficient and concentration [35].

Calibration of Observation Volume

The effective volume element (V_{eff}) is defined by the point spread function (PSF) of the system and defined by:

$$V_{eff} = \frac{\int PSF(r) dr}{PSF(0)} \quad (9)$$

where PSF(r) is the PSF at the location r in the image plane. For a three-dimensional Gaussian laser beam profile in radial and axial direction, this effective volume calculates as:

$$V_{eff,3DG} = \pi^{3/2} \cdot r_0^2 \cdot z_0 \quad (10)$$

r_0 can be conveniently determined by measuring the diffusion time τ_D of a molecule with defined diffusion coefficient D by fitting the data to a free 3-D translational diffusion model (see Table 4):

$$\tau_D = \frac{r_0^2}{4D} \quad (11)$$

From the same fit the structural parameter (S) can be used to calculate z_0 :

$$S = \frac{z_0}{r_0} \quad (12)$$

The autocorrelation data must be of the highest quality in order to obtain reliable values. Therefore, only photostable bright dyes should be used for the calibration procedure. Rhodamine 6G ($D=2.8 \times 10^{-10} \text{ m}^2/\text{sec}$) and Cy5 ($D=3.16 \times 10^{-10} \text{ m}^2/\text{s}$) work well in determining the effective volumes for the 488 nm and 633 nm lines, respectively. It should be noted that the ratio of the volumes for different wavelengths are proportional to the third power of the wavelength ratios:

$$\frac{V_r}{V_b} = \left(\frac{\lambda_r}{\lambda_b} \right)^3 \quad (13)$$

Calculations of the PSF give a structural parameter between 2 and 3 [35]. However, in most calibration measurements, the structural parameter will be 5 to 5.5 for the 488 nm line, and 8 to 8.5 for the 633 nm line with the ConfoCor 2. These higher values are due to optical aberrations and are also found with other FCS systems [35].

Once the dimensions of the observation volume are known, the information can be used to calculate the diffusion coefficients of the molecules under investigation according to equation 11. For cross-correlation experiments $\tau_{D,rg}$ represents the weighted diffusion time of the double-labelled molecules N_{rg} :

$$\tau_{D,rg} = \frac{r_{0,rg}^2 + r_{0,r}^2}{8D} \quad (14)$$

and the effective volume element is defined by:

$$V_{eff,rg} = \left(\frac{\pi}{2} \right)^{3/2} \cdot (r_{0,g}^2 + r_{0,r}^2) \cdot (z_{0,g}^2 + z_{0,r}^2)^{1/2} \quad (15)$$

Calibration of Concentrations

The autocorrelation amplitude $G(0)$ is inversely proportional to the number N and hence concentration c of the molecules:

$$G(0) = 1 + \frac{\gamma}{N} \quad (16)$$

γ is a factor that accounts for the form of the PSF [36].

The upper limit of useful concentrations is determined by the instrumental noise, which will dominate as autocorrelation amplitudes decrease. There is also a lower limit of observable concentrations, since at low count rates with highly diluted samples, background counts can become significant. The concentration (c) in the sample can be calculated according to:

$$c = \frac{N}{V_{eff} \cdot N_A} \quad (17)$$

where N is the average number of molecules, V_{eff} the effective volume element, and $N_A = 6.023 \times 10^{23} \text{ mol}^{-1}$, Avogadro's number. To determine N one needs to know the factor γ . By using a defined concentration of a dye this factor can be determined according to:

$$\gamma = [G(0) - 1] \cdot c \cdot V_{eff} \cdot N_A \quad (18)$$

The concentration of the dye can be accurately measured by absorption spectroscopy using the Lambert-Beer equation:

$$A = c \cdot l \cdot \epsilon \quad (19)$$

A , l , c and ϵ representing the absorption value, the absorption path length (cm), the molar absorption coefficient ($\text{l mol}^{-1} \text{ cm}^{-1}$) of the dye and the concentration (mol l^{-1}). Since FCS requires substantially lower amounts than adsorption spectrometry, a dilution series of the dye has to be prepared for calibration of the ConfoCor 2.

Often, as also applies to the ConfoCor 2 software, the factor γ is set at a fixed value of 1. Such a value is consistent with a PSF which is constant within a volume element, and zero outside it, such as a cylindrical shaped volume, and can be used as an approximation for the effective volume element under certain conditions [19]. This simplification can be conveniently used if the concern is not absolute, but rather relative concentrations.

Calibration of Molecular Brightness

The molecular brightness η describes the detected fluorescence intensity of a single molecule. It is calculated by the ConfoCor 2 software by dividing the mean fluorescence intensity by the mean number of molecules, and hence its unit is given as counts per s and molecule (cpsm), preferentially referred to as the counts per molecule (cpm):

$$\eta = \frac{\langle I \rangle}{\langle N \rangle} \quad (20)$$

η varies with the laser power and concentration of the sample [1], but it also depends on the properties of the dye and instrumental properties such as optical filters, quantum yield of the detectors and microscope optics. If the same conditions are used, the molecular brightness is a useful parameter for checking the system's performance. It is advisable to check the molecular brightness of a standard sample at a defined laser power and concentration once in a while. A reduction in brightness indicates problems with the instrument.

The molecular brightness can change if a molecule binds to another molecule or if a molecule encounters a different environment. The square of the brightness of each species contributes to the correlation curve (see Table 3). This means that a species with twice the brightness contributes 4-fold more to the correlation function, and if possible, such changes in brightness should be taken into account. Changes can either be determined by absorption spectroscopy, if all partners are available in a soluble form and in sufficient quantities, or by analysis of the experiment with a photon counting histogram (PCH) or fluorescence intensity distribution analysis (FIDA) [37, 38].

Single Molecule Analysis

Using the confocal volume element signal-to-background ratios in the range of 1000:1 and above can be obtained [39, 40]. This opens the possibility of single molecule detection and spectroscopy for chemical and biochemical systems. Single molecule analysis in combination with FCS has been successfully used for the analysis of enzymatic catalysis [41]. A single enzyme attached to a glass surface that bears a label or is indirectly marked by binding to a fluorescent substrate or product can be easily imaged by scanning over the area of interest with the piezo stage. Once in the laser focus conformational kinetics of a single molecule can be measured [42, 43]. For a detailed kinetic analysis of correlation curves the reader is referred to the literature [41].

Not only immobilised molecules can be investigated on a single base, but diffusing molecules as well. Although FCS in its normal application is single-molecule sensitive, the obtained parameters are the average signal of many molecules. However, a single burst of photons originating from one molecule can be analysed from the raw data trace to obtain information about a single molecule [44-47]. Also algorithms have been developed, called Single (solution)-Phase Single-Molecule FCS (SPSM-FCS) that allows the continuous observation of the same single molecule in solution and a membrane for extended periods of time, i.e. form (milli)-seconds up to several hours [48, 49, 66-68].

EXPERIMENTAL SET-UP FOR PHARMACOLOGICAL STUDIES

Classical approaches to studying ligand-receptor interactions have involved radioactive labelling of the ligands. With

this approach larger quantities of cells have to be screened. However, often, such as with primary cell cultures or biopsies, cultures are slow growing or differentiated and heterogeneous. Culturing of such cells in artificial media often results in time-dependent changes in cell phenotype. Such conditions require a technique which is more sensitive yet still quantitative at a single cell level. The advantage of FCS lies in its non-invasive character, meaning this technique can not only be used in solution but also in a cell or its membrane [16, 18, 50]. A free ligand can easily be distinguished from one bound to a receptor due to its faster diffusion time: the difference is generally more than the required 1.6-fold, which corresponds to a mass difference of at least 5-fold [27]. Moreover, FCS allows the number of free and bound particles to be determined in one measurement in the direct vicinity of the receptor. Therefore the kinetics of a reaction can be determined for single cells. Furthermore, membrane receptors are no longer thought to exist uniformly distributed throughout the cell membrane, but are localised in highly ordered and specialised membrane domains, such as caveolae or cholesterol-rich lipid rafts. Classic techniques do not yield information on the pharmacology of receptors within these domains, and it is here that single molecule technologies such as FCS have come of age. We will focus here on ligands binding to cell surface receptors.

Practical Considerations for Cellular Studies

FCS measurements in living cells suffer from a lower SNR compared to solution measurements. Structures in the cell can lead to scattered excitation and emission light. To some extent, the SNR can be improved by increasing the excitation power, however, care must be taken to avoid bleaching artefacts. Cells are small compartments, which limits the supply of fresh dye molecules. Therefore, a compromise has to be reached between a high molecular brightness and minimized contributions of photobleaching and cell damage. The SNR can be improved with elongated measurement times. However, this again can cause more extensive sample bleaching and longer measurement times suffer from the risk of fluctuations arising from organelle or cell movement [11]. Autofluorescence or other background fluorescence can contribute to the correlation curve either as a constant, non-correlating species, lowering the correlation amplitude by a factor $(1-I_b/I_s)$, or as an additional correlating component. The first contribution can be easily corrected for, if the background is determined in cells expressing no label. The latter will require determining the brightness of the autofluorescence and hence its contribution to the correlation function. If significant, this contribution has to be accounted for by a second species in the fit. In the case of similar diffusion times, however, the system will not be able to discriminate between autofluorescence and the true signal. One should also keep in mind, that the metabolic state of a cell not only has a strong influence on the brightness of the autofluorescence, but also on a labelled molecule [51]. At low pH values GFP undergoes a photophysical process called blinking or flickering [52]. In this case, a second exponential function has to be incorporated into the fit model.

Taking Measurements on the Cell Membrane

Using auto-correlation measurements, it is the ligand that should be labelled, since free and bound forms can be distinguished easily. Naturally, the pharmacological performance of the labelled ligand has to be checked in comparison to the unlabelled form. Normally, labelling is done chemically, and is preferably with a photostable dye of high quantum yield. For cellular work, the physicochemical properties of the dye can also substantially affect the properties of the ligand. For instance, rhodamine-based dyes bind well to most cell membranes in a non-specific manner, and may introduce a high degree of non-specific binding. Other dyes are particularly lipophilic and may rapidly accumulate in the cytoplasm. It is also preferable to check the photophysical properties of the labelled ligand, since chemical modification of the pharmacophore may alter excitation and emission maxima and quantum yield. In particular, many high quantum yield fluorophores become far less efficient in the aqueous environment needed for experiments on live cells. For a number of reasons, red-shifted fluorophores may be preferable for ligand binding experiments. Autofluorescence and phototoxicity are substantially reduced at 633nm compared to 488 or even 543nm and triplet state formation tends to be lower in red-excited dyes. Finally, since no red shift monomeric GFP-derivatives are available on the market as yet, it is recommended that the ligand is labelled with a dye easily excited by the 633 nm line if cross-correlation experiments are planned using GFP-tagged receptors.

With respect to ligand design, labelling of peptide ligands with an appropriate amine-reactive fluorophore is relatively straightforward. Since the ligand is large relative to the label, gross changes in pharmacology are less likely. However, structure-activity relationships (SARs) for the ligand should still be consulted to check that a crucial residue is not being targeted. For small molecule ligands, the situation is more complex and is dependent entirely on the receptor-ligand pair of interest. For instance, for G-protein coupled receptors with small molecule ligands, the fluorophore is often of the same size as the pharmacophore, and the binding site is

form. Fixing of this parameter in later experiments will aid curve-fitting. If the K_d is high, as determined in pharmacological assays, one may be forced to add unlabelled molecules in order to obtain a concentration range where binding occurs. However, especially when the labelled ligand has a different affinity to the receptor, evaluation can be quite complicated. The concentration of the labelled ligand should not exceed 10^{-7} M, otherwise correlation amplitudes become too small. Alternatively, competition, rather than saturation binding assays should be considered, if there is a suitable high affinity unlabelled ligand available. In the case of kinetic experiments algorithms have become available that allow the determination of binding constants at substrate concentrations well below the Michaelis-Menton constant [53].

Next, the ligand is added to the medium of cells that express the receptor of interest. After reaching equilibrium, the labelled cells are imaged via LSM and positioned either manually using a crosshair or by stage movement by setting a cross in the image. Once positioned the membrane is detected via a Z-scan. If the ligand binds to its receptor or the receptor itself is labeled, two peaks should usually be visible in the scan, corresponding to the lower and the upper membrane (Fig. (7)). This separation is most prominent if the scan is performed at a location where the nucleus is present. Depending on the ligand properties, the lower membrane, however, might not be visible. The position of the confocal volume is then defined by the bar in the scan window. This can be the peak itself, or, if one wishes to avoid the cytoplasm as much as possible, the volume can be positioned slightly higher, which, however, results in lower signals and different diffusion times [15, 54]. Whichever position is chosen, it should be placed consistently in each experiments. Inconsistency results in variations in the estimation of free ligand concentration, which may be as much as 2-fold. When the volume element is positioned onto the cell surface, not only the bound ligand diffusing at the cell surface, but also unbound ligand diffusing above the cell surface will be seen. Then the auto-correlation function will be a combination of the 3-D diffusion of the free and 2-D diffusion of the bound ligand and is given by [55, 56]:

$$G(\tau) = 1 + \frac{1}{N} \left[f_f \cdot \eta_f^2 \cdot \left(\frac{1}{1 + \tau/\tau_{D,f}} \right) \cdot \left(\frac{1}{1 + \tau/\tau_{D,f} \cdot S^{-2}} \right)^{1/2} + f_b \cdot \eta_b^2 \cdot \left(\frac{1}{1 + \tau/\tau_{D,b}} \right) \right] \quad (21)$$

within the membrane domains of the receptor. Careful study of SARs will give some insight into the appropriate labelling strategies. For instance, incorporation of a linker to separate fluorophore from the binding moiety may maintain ligand affinity.

In the first step, the ligand is characterised in solution. This allows determination of the diffusion time of the free

where η_f and η_b are the quantum yields or molecular brightnesses of the free and bound ligand diffusing with diffusion times $\tau_{D,f}$ and $\tau_{D,b}$ and fractional concentrations f_f and f_b ($f_f + f_b = 1$).

It is recommended to use the upper membrane for measurements to avoid any reflected light possibly generated by glass reflection if the volume is positioned in the lower

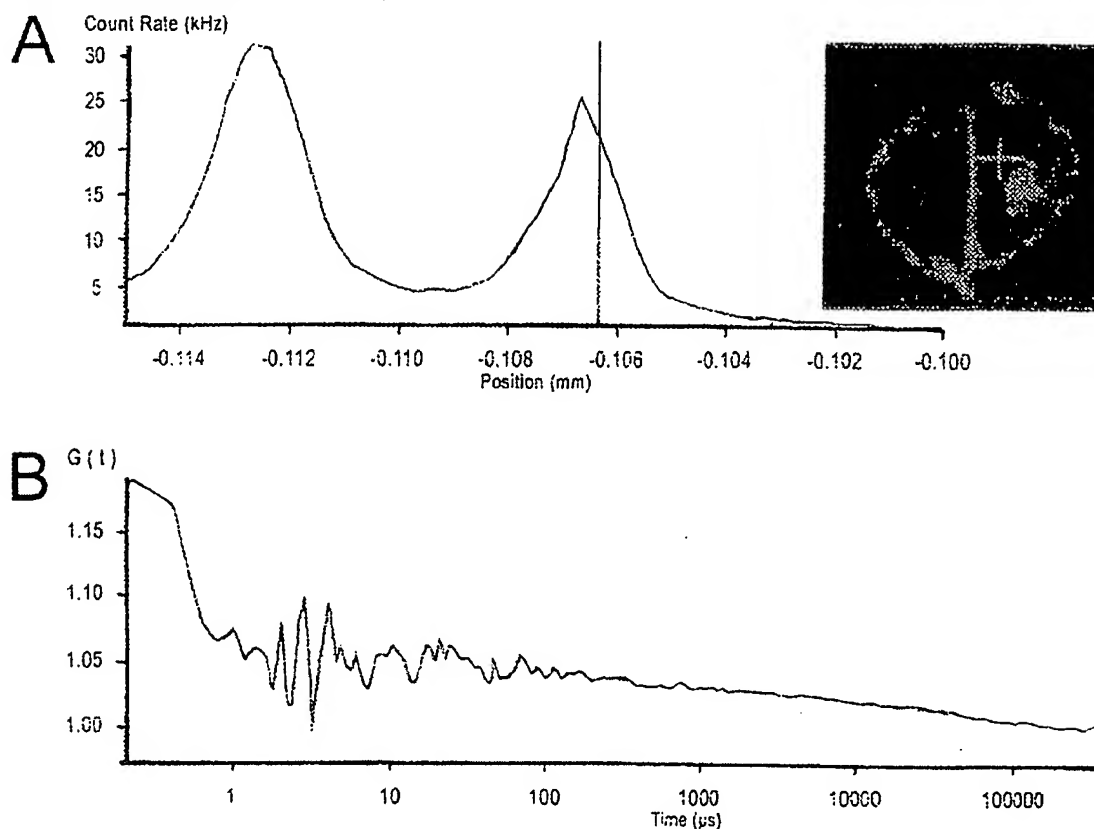


Fig. (7). Positioning of the confocal volume on a cell membrane (z-Scan, panel A) and auto-correlation function obtained for a GFP coupled receptor (panel B).

membrane. The lower membrane, especially at sites where the cell attaches to its substrate, might also be less or even not at all accessible for the ligand, leading to anomalous kinetics. It is also advisable to approach the membrane from the top of the cell and not from the side, due to the shape of the confocal volume – this results in a much clearer membrane definition in the Z-scan. To avoid reflections during the scan, the laser module is equipped with shutters and line filters that effectively block all the laser lines not in use. In addition, the laser intensity can be drastically reduced to lessen bleaching of the sample during the scan.

Once correctly positioned, measurements can be triggered. A first set of experiments should aim to determine the approximate diffusion time of the receptor or bound ligand. For further experiments, measurement times should be chosen that are approximately 1000-fold longer than the diffusion time, since FCS is a statistical method and requires approximately 1000 transits of the molecule to be statistically significant. Alternatively, if bleaching becomes a problem, measurement times can be reduced and measurements repeated more often to obtain the same overall acquisition time. For this reason, the ConfoCor 2 software offers the possibility of averaging the correlation results instead of the single parameters. If multiple measurements are taken it can be advantageous to export the data and fit them globally [57]. This will yield more stable fit parameters. However, it

should be kept in mind, that with a measuring regime using repeated shorter acquisition times the statistics are inferior compared to taking one measurement with a longer time [58]. Especially when dealing with over-expressing cells, one often sees bleaching in the first measurements taken. This bleaching may be due to one of two reasons: first, slow or immobile molecules that are bleached preferentially, and second, since the laser beam is stationary high local concentrations of singlet oxygen may be created. Immobilisation often occurs in over-expressed systems since the molecules will bind unspecifically to cellular structures. If one wants to avoid bleaching curves, the ConfoCor 2 can incorporate a pre-bleaching step with an arbitrary laser power.

Whereas the external addition of ligand can be precisely controlled in terms of molecules added, internal expression of GFP-fusion proteins often relies on strong promoters such as the CMV promoter. In this case, one has to screen freshly transfected cells or unselected stable cell lines for low expressors. This is, of course, a compromise as autofluorescence is higher with 488nm excitation, and the expression level needs to be sufficient that a count rate of at least 10-fold above background is obtained at a relatively low laser power. If high concentrations become a problem there is still the option of pre-bleaching the sample. For this purpose, the LSM should be used and the high laser intensities used for efficient bleaching should be evenly distributed over the area

of the cell. In contrast, FCS only permits spot bleaching, and this can lead to more rapid damage to the cell. A typical auto-correlation measurement of GFP-tagged receptor is shown in Fig. (7).

In contrast to bulk bleaching, which is mainly due to light outside the focal plane, bleaching can also occur in the confocal volume element. Bulk bleaching will lead to a decrease in the overall count rate and to a drop in the correlation curve to below 1. If the drop is continuous, i.e. the curve does not level off at 1 before the drop, in other words the curve is divergent, this will lead to an artificial increase in diffusion times, since such a drop can trail into, and influence the transition in the curve caused by the real diffusion of the molecule. Spot bleaching, in contrast, will not lead to a substantial reduction of the count rate, but will affect the diffusion time. In this case diffusion times become faster, since a bleached molecule is considered to have moved out of the volume element. To ensure that spot bleaching is not an issue, the laser power should initially be set as low as possible while still obtaining a sufficient SNR, i.e. cpm value. In control experiments one should systematically vary the laser power and observe when the molecules seem to speed up [18].

In ligand-receptor binding studies the ligand has to be present in the media if dissociation constants are to be determined. However, in situations studying receptor oligomerisation upon ligand binding or uptake of the ligand, one can often wash the cells free of the unbound, non-incorporated ligand, which will make it easier to fit the data

determined and this parameter fixed in the fit. It is evident that the accuracy of fitting is inversely related to the number of parameters that have to be fixed.

The correlation analysis links diffusion times and numbers of particles with direct readouts. This can be easily transformed into diffusion coefficients and concentrations, knowing the dimensions of the confocal volume element, which should be determined beforehand with free dye solutions.

The diffusion times reveal information about binding events and diffusional characteristics of the receptor-ligand complex in the membrane, whereas concentrations can be used to determine kinetic parameters of the system.

Converting FCS Data Into Pharmacologically Relevant Values

For the analysis of ligand-receptor binding on the cell surface we assume a membrane surface containing receptors with a total concentration of $[R]_0$ [56]. If ligand is added to the medium at a total concentration $[L]_0$, it will fractionally bind to the receptor until equilibrium is reached between bound ($[L]_b = [LR]$) and free ligand ($[L]_f$). Hence, $[L]_0 = [L]_f + [L]_b = [L]_f + [LR]$ and $[R]_0 = [R]_f + [R]_b = [R]_f + [LR]$.

If the diffusion time, τ_D , of the ligand is much faster than the chemical relaxation time $\tau_{chem} = (k_{ass} + k_{diss})^{-1}$ and the quantum yield does not change upon ligand binding, equation 21 simplifies to

$$G(\tau) = 1 + \frac{1}{N} \left[f_f \cdot \left(\frac{1}{1 + \tau/\tau_{D,f}} \right) \cdot \left(\frac{1}{1 + \tau/\tau_{D,f} \cdot S^{-2}} \right)^{1/2} + f_b \cdot \left(\frac{1}{1 + \tau/\tau_{D,b}} \right) \right] \quad (22)$$

later. The success of this approach will very much depend on the kinetics of the ligand used.

Evaluation of the Data

Once sufficient measurements have been taken, the data have to be fitted to an appropriate model. Table 3 lists common diffusion models. Models for rotational diffusion, antibunching and translational diffusion in the presence of barriers and membranes are available as well [45, 59-65]. Although the ConfoCor 2 fit software is modelled for a 3-D, free-diffusion process, the structural parameter can be set to high values to obtain a 2-D fit. However, a 3-D fit often also works for membranes, and the preferred option depends on the user. Only convergent curves, i.e. those that level off around 1, regardless of whether there is a rise or drop at later correlation times, should be taken into account for analysis. One should first start with a one-component system and only if this does not give a satisfactory fit, should one proceed to more components. It is also a good idea to characterise the system as accurately as possible in preliminary experiments. For example, the diffusion time of the free ligand can be

where N is the total number of labelled ligand and hence $[L]_0 = N/V$, $[LR] = f_b \cdot N/V = f_b \cdot [L]_0$, and $[L]_f = f_f \cdot N/V = (1 - f_b) \cdot [L]_0$.

In traditional drug-receptor interaction analysis, the binding capacity (number of receptors), the dissociation constant for the ligand (K_d), and the on and off-rates of binding are all accessible providing that the appropriate values for free and bound ligand are known. Thus FCS measurements make it possible to calculate these values for a fluorescently labelled ligand at a single cell level. However, in most cases, measurements will need to be taken at a range of either ligand or competitor ligand concentrations. The method of choice will depend on the properties of the ligand of interest. A brief outline of this analysis follows, although the reader is referred to a more thorough text for full explanation of the analysis [66].

Basic analysis of ligand receptor interaction is based on a simple reversible uni-molecular interaction between drug and receptor to form a drug-receptor complex. The assumption is made that ligand-receptor interaction occurs when a single ligand molecule interacts with a receptor in the correct orientation with enough energy to bind.



According to the Law of Mass Action, the forward (association) rate and reverse (dissociation) rate are given by:

$$\text{forward} = k_{on} \cdot [L]_f \cdot [R]_f \text{ and } \text{reverse} = k_{off} \cdot [LR] \quad (24 \text{ a,b})$$

where the angular brackets represent concentration terms. At equilibrium, these rates will be equal, which allows the dissociation constant to be defined as:

$$K_d = \frac{k_{off}}{k_{on}} = \frac{[L]_f \cdot [R]_f}{[LR]} \quad (25)$$

For determination of K_d , it is therefore necessary to know the number of unoccupied receptors $[R]_f$, which we cannot measure. However, since the total number of receptors $[R]_0$ is equal to occupied $[LR]$ plus unoccupied $[R]$, the above equation can be rearranged to give:

$$K_d = \frac{[L]_f \cdot ([R]_0 - [LR])}{[LR]} \quad (26)$$

Rearrangement of this gives a form of the familiar Hill-Langmuir binding isotherm:

$$[LR] = \frac{[L]_f \cdot [R]_0}{K_d + [L]_f} \quad (27)$$

In terms of parameters obtained by FCS equation (27) can be rewritten as

$$f_b \cdot [L]_0 = \frac{(1 - f_b) \cdot [L]_0 \cdot [R]_0}{K_d + (1 - f_b) \cdot [L]_0} \quad (28)$$

It is evident from this that determination of K_d from a single measurement of free $[L]_f$ and bound $[LR]$ concentrations is not possible, since the binding capacity, $[R]_0$ is not known. Thus, bound concentrations over a range of free ligand concentrations need to be determined. A subsequent plot of free concentration against bound will yield a binding hyperbola. Non-linear regression analysis of this curve will yield values for R_0 , which is the asymptote on the y-axis, and K_d , which is the free concentration at which 50% of R_0 is achieved (i.e. half the receptors are occupied). It should be noted that herein lies one of the major advantages of FCS analysis, that the actual free concentration of ligand is measured, whereas in radioligand binding analysis, the free concentration of ligand is assumed to be the same as that added, i.e. there is no ligand depletion or partitioning within the reaction vessel. This can lead to errors in affinity measurements, which are particularly large at low ligand concentrations. However, this also illustrates one problem of ligand design for FCS. For regression analysis, occupancy of the receptor needs to be high, to achieve saturation and subsequently determine the binding capacity accurately. To achieve this, the free concentration needs to be increased to 5-fold and preferably 10-fold above the K_d value. Since concentrations of greater than 100nM are difficult to

measure with FCS, this means ligands should have K_d values of less than 20-30nM for accurate saturation analysis.

Generally speaking, total binding of a ligand is not saturable, as it consists of both specific binding (to the receptor) and non-specific binding (to the membrane, non-receptor proteins etc.). Non-specific binding can be determined by measuring binding in the presence of a saturating concentration of a non-fluorescent high affinity receptor ligand (100-1000-fold K_d). Non-specific binding usually increases linearly with ligand concentration. Specific binding is simply defined as total binding minus non-specific.

Some of these problems may be surmounted by using competition binding assays. This approach will not provide a K_d for the fluorescent ligand, but will still allow pharmacological characterisation of the receptor using the known affinity of a previously characterised ligand. Again, the assay relies on reversible binding of both label and competitor at equilibrium. In this instance, a fixed concentration of fluorescent ligand is incubated with increasing concentrations of an unlabelled ligand. This is described as follows:

$$[L]_X = \text{NSB} + \frac{([L]_T - \text{NSB})}{1 + 10^{X/IC_{50}}} \quad (29)$$

where $[L]_X$ is the amount of bound ligand in the presence of a concentration $[X]$ of competing ligand, NSB is the non-specific binding, $[L]_T$ is the amount of ligand binding in the absence of competing ligand, and IC_{50} is the concentration of competitor causing a 50% reduction in the amount of specific binding of labelled ligand. A plot of $\log [X]$ vs $[L]_X$ results in a sigmoidal decay curve from which all of the other parameters can be determined using non-linear regression. The value for IC_{50} obtained from this equation is not the affinity value for the competing drug, since the value will depend on the concentration of labelled ligand used. The IC_{50} can be corrected to an affinity value, K_i using the Cheng-Prusoff equation for pure competition at a single site [67]:

$$K_i = \frac{IC_{50}}{1 + \frac{[L]_T}{K_d}} \quad (30)$$

This equation allows K_i , the affinity value of the competing ligand, to be calculated from the IC_{50} value, the concentration, $[L]_T$, of labelled ligand and K_d , the affinity value for the labelled ligand. If saturation binding is not possible, this K_d value should be one estimated from pharmacological assays.

CONCLUSIONS

Fluorescence correlation spectroscopy has come of age for cell biological applications. Its confocal setup makes it complementary to many other fluorescence techniques and guarantees a high spatial resolution. Useful pharmacological parameters can be determined under thermodynamic equilibrium like kinetic and binding constants. Accessible time scales range from sub-microseconds to several hundred milliseconds rendering the method suitable to study ligand-

receptor interactions. Technical advances, the development of new powerful software tools and improvements in fluorescent dyes doubtless will open new avenues using FCS in single-molecule detection and in *in vivo* pharmacological investigations.

ACKNOWLEDGEMENT

The authors want to thank Anne Kenworthy for pointing out bleaching strategies to reduce the number of fluorescent particles, John Carson and Anne Cowen for their discussion of bleaching artefacts and Mark Hink for helpful support in defining the optical performance of the instrument.

REFERENCES

- [1] Jankowski, T. and R. Janka, ConfoCor2 - The Second Generation of Fluorescence Correlation microscopes, in *Fluorescence Correlation Spectroscopy: Theory and Applications*, R. Rigler and E.L. Elson, Editors. 2001, Springer: Berlin Heidelberg, p. 331-345.
- [2] Starr, T.E. and Thompson, N.L. (2001) *Biophys. J.*, 80(3), p. 1575-84.
- [3] Brinkmeier, M., Doerrie, K., Stepanh, J. and Eigen, M. (1999) *Anal. Chem.*, 71(3), p. 609-616.
- [4] Chang, I.C. (1981) *Optical Engineering*, 20, p. 824-829.
- [5] Dickinson, M.E., Bearman, G., Tilie, S., Lansford, R. and Fraser, S.E. (2001) *Biotechniques*, 31(6), p. 1272, 1274-6, 1278.
- [6] Lansford, R., Bearman, G. and Fraser, S.E. (2001) *J. Biomed. Opt.*, 6(3), p. 311-8.
- [7] Rigler, R., Foldes-Papp, Z., Meyer-Almes, F.J., Sammet, C., Volcker M. and Schnetz, A. (1998) *J. Biotechnol.*, 63(2), p. 97-109.
- [8] Wachsmuth, M., Weidemann, T., Muller, G., Hoffmann-Rohrer, U.W., Knoch, T.A., Waldeck, W. and Langowski, J. (2003) *Biophys. J.*, 84(5), p. 3353-63.
- [9] Palmer, A.G. 3rd and Thompson, N.L. (1989) *Proc. Natl. Acad. Sci. USA*, 86(16), p. 6148-52.
- [10] Widengren, J. and Rigler, R. (1998) *Cell. Mol. Biol. (Noisy-le-grand)*, 44(5), p. 857-79.
- [11] Hink, M.A., Bors, J.W. and Visser, A.J. (2003) *Methods Enzymol*, 361, p. 93-112.
- [12] Aragón, S.R. and Pecora, R. (1976) *J. Chem. Phys.*, 64, p. 1791-1803.
- [13] Elson, E.L. and Magde, D. (1974) *Biopolymers*, 13, p. 29.
- [14] Magde, D.E., E. L. (1974) *Biopolymers*, 13, p. 29.
- [15] Schwill, P., Haupts, U., Maiti S. and Webb, W.W. (1999) *Biophys. J.*, 77(4), p. 2251-65.
- [16] Schwill, P., Korfach, J. and Webb, W.W. (1999) *Cytometry*, 36(3), p. 176-82.
- [17] Widengren, J.D., Rigler, R. (1995) *J. Phys. Chem.*, 99(36), p. 13368.
- [18] Bacia, K. and Schwill, P. (2003) *Methods*, 29(1), p. 74-85.
- [19] Rigler, R., Mets, U., Widengren, J. and Kask, P. (1993) *Eur. Biophys. J.*, 22, p. 169.
- [20] Wohland, T., Rigler, R. and Vogel, H. (2001) *Biophys. J.*, 80(6), p. 2987-99.
- [21] Qian, H. and Elson, E.L. (1991) *Appl. Optics*, 30, p. 1185-1195.
- [22] Hess, S.T. and Webb, W.W. (2002) *Biophys. J.*, 83(4), p. 2300-17.
- [23] Marquardt, D.W. (1963) *J. Soc. Ind. Appl. Math.*, 11, p. 431-441.
- [24] Press, W.H., Teukolsky, S.A., Vetterling, W.T. and Flannery, B.P. in *Numerical Recipes in C*, 1995, Cambridge University Press, Cambridge.
- [25] Apasnovich, V.V. and Novikov, E.G. (1990) *Optics Commun.*, 78(279-282).
- [26] Novikov, E.G., van Hoek, A., Visser, A.J.W.G. and Hofstra, J.W. (1999) *Opt. Commun.*, 166, p. 139.
- [27] Meseth, U., Wohland, T., Rigler, R. and Vogel, H. (1999) *Biophys. J.*, 76(3), p. 1619-31.
- [28] Koppel, D. (1974) *Phys. Rev. A*, 10, p. 1938-1945.
- [29] Brock, R. and Jovin, T.M. *Fluorescence Correlation Microscopy (FCM): Fluorescence Correlation Spectroscopy (FCS) in Cell Biology*, in *Fluorescence Correlation Spectroscopy: Theory and Applications*, R. Rigler and E.L. Elson, Editors. 2001, Springer: Berlin Heidelberg, p. 132-161.
- [30] Schwill, P. (2001) *Cell Biochem. Biophys.*, 34(3), p. 383-408.
- [31] Ketting, U., Koltermann, A., Schwill, P. and Eigen, M. (1998) *Proc. Natl. Acad. Sci. USA*, 95(4), p. 1416-20.
- [32] Schwill, P., Bieschke, J. and Ochenschlager, F. (1997) *Biophys. Chem.*, 66(2-3), p. 211-23.
- [33] Schwill, P., Meyer-Almes, F.J. and Rigler, R. (1997) *Biophys. J.*, 72(4), p. 1878-86.
- [34] Bacia, K., Majoul, I.V. and Schwill, P. (2002) *Biophys. J.*, 83(2), p. 1184-1193.
- [35] Mueller, J.D., Chen, Y. and Gratton, E. (2003) *Methods Enzymol*, 361, p. 69-92.
- [36] Thompson, N.L., *Fluorescence Correlation Spectroscopy*, Topics in Fluorescence Spectroscopy, ed. J.R. Lakowski, Vol. 1, 1991, New York: Plenum Press.
- [37] Chen, Y., Muller, J.D., So, P.T. and Gratton, E. (1999) *Biophys. J.*, 77(1), p. 553-67.
- [38] Kask, P. and Palo, K. Introduction to the Theory of Fluorescence Intensity Distribution Analysis, in *Fluorescence Correlation Spectroscopy: Theory and Applications*, R. Rigler and E.L. Elson, Editors. 2001, Springer: Berlin Heidelberg, p. 396-409.
- [39] Rigler, R. and Mets, U. (1993) *Soc. Photo-Opt. Instrum. Eng.*, 1921, p. 239-248.
- [40] Mets, U. and Rigler, R. (1994) *J. Fluorescence*, 4(3), p. 259-264.
- [41] Rigler, R., Wennmalm, S. and Edman, L. FCS in Single Molecule Analysis, in *Fluorescence Correlation Spectroscopy: Theory and Applications*, R. Rigler and E.L. Elson, Editors. 2001, Springer: Berlin Heidelberg, p. 459-476.
- [42] Edman, L., Mets, U. and Rigler, R. (1996) *Proc. Natl. Acad. Sci. USA*, 93(13), p. 6710-5.
- [43] Wennmalm, S., Edman, L. and Rigler, R. (1997) *Proc. Natl. Acad. Sci. USA*, 94(20), p. 10641-6.
- [44] Keller, R.A., Ambrose, W.P., Goodwin, P.M., Jet, J.H., Martin, J.C. and Wu, M. (1996) *Appl. Spectrosc.*, 50, p. 12A-32A.
- [45] Eggeling, C., Fries, J.R., Brand, L., Gunther, R. and Seidel, C.A. (1998) *Proc. Natl. Acad. Sci. USA*, 95(4), p. 1556-61.
- [46] Fries, J.R., Brand, L., Eggeling, C., Koellner, M. and Seidel, C.A.M. (1998) *J. Phys. Chem. A*, 102, p. 6601-6613.
- [47] Schaffer, J., Volkmer, A., Eggeling, C., Subramanian, V., Striker, G. and Seidel, C.A.M. (1999) *J. Chem. Phys. A*, 103, p. 331-336.
- [48] Foldes-Papp, Z., Demel, U. and Tilz, G.P. (2002) *J. Immunol. Methods*, 260(1-2), p. 117-24.
- [49] Foldes-Papp, Z., Demel, U., Domej, W. and Tilz, G.P. (2002) *Exp. Biol. Med. (Maywood)*, 227(5), p. 291-300.
- [50] Sengupta, P., Garai, K., Balaji, J., Perisiamy, N. and Maiti, S. (2003) *Biophys. J.*, 84(3), p. 1977-84.
- [51] Brock, R., Hink, M.A. and Jovin, T.M. (1998) *Biophys. J.*, 75(5), p. 2547-57.
- [52] Schwill, P., Kummer, S., Heikul, A.A., Moerner, W.E. and Webb, W.W. (2000) *Proc. Natl. Acad. Sci. USA*, 97(1), p. 151-6.
- [53] Meyer-Almes, F.J. and Auer, M. (2000) *Biochemistry*, 39(43), p. 13261-8.
- [54] Benda, A., Benes, M., Thermer, W.T. and Hof, M. (2003) *Langmuir*, 19(10), p. 4120-4126.
- [55] Rigler, R., Pramanik, A., Jonasson, P., Kratz, G., Jansson, O.T., Nygren, P., Stahl, S., Ekberg, K., Johansson, H., Uhlen, S., Uhlen, M., Jomvall, H. and Wahren, J. (1999) *Proc. Natl. Acad. Sci. USA*, 96(23), p. 13318-23.
- [56] Pramanik, A. and Rigler, R. (2001) *Biol. Chem.*, 382(3), p. 371-8.
- [57] Beechen, J.M., Gratton, E., Ameloot, M., Knutson, J.R. and Brand, L. The global analysis of fluorescence intensity and anisotropy decay data: second-generation theory and programs, in *Topics in Fluorescence Spectroscopy*, J.R. Lakowicz, Editor. 1992, Plenum Press: New York, p. 241.
- [58] Saffarian, S. and Elson, E.L. (2003) *Biophys. J.*, 84(3), p. 2030-42.
- [59] Ehrenberg, M. and Rigler, R. (1974) *Chem. Phys.*, 13, p. 29-61.
- [60] Kask, P., Pikkars, P., Mets, U., Pooga, M. and Lippman, E. (1987) *Eur. Biophys. J.*, 14(4), p. 257-61.
- [61] Widengren, J., Mets, U. and Rigler, R. (1999) *Chem. Phys.*, 250(2), p. 171-186.
- [62] Mets, U., Antibunching and Rotational Diffusion in FCS, in *Fluorescence Correlation Spectroscopy: Theory and Applications*,

- R. Rigler and E.L. Elson, Editors. 2001, Springer: Berlin Heidelberg. p. 346-359.
- [63] Gennerich, A. and Schild, D. (2000) *Biophys. J.*, 79(6), p. 3294-306.
- [64] Gennerich, A. and Schild, D. (2002) *Biophys. J.*, 83(1), p. 510-22.
- [65] Weiss, M., Hashimoto, H. and Nilsson, T. (2003) *Biophys. J.*, 84(6), p. 4043-52.
- [66] Kenakin, T. *Pharmacologic Analysis of Drug Receptor Interaction*. 2 nd ed. 1993, Raven press.
- [67] Cheng, Y. and Prusoff, W.H. (1973) *Biochem. Pharmacol.*, 22(23), p. 3099-108.
- [68] Földes-Papp, Z. (2002) *Pteridines*, 13, 73-82.
- [69] Földes-Papp, Z., Demel, U., Titz, G.P. (2004) *J. Immunol. Meth.*, in press.
- [70] Földes-Papp, Z., Demel, U., Titz, G.P. (2004) *J. Immunol. Meth.*, in press.



Division
Advanced Imaging Microscopy
Carl Zeiss Jena GmbH, 07740 Jena

Original:

CARL ZEISS, Inc.
--Acc. Dept., Mrs. I. Driscoll--
One Zeiss Drive
THORNWOOD NY 10594
USA

Invoice

Please always indicate:
Division/Number/Date
45/2040118607/08/10/2000

Contact
Nancy Vogel
Phone/Fax
(03641) 64 3138 / 64 3139
e-mail
n.vogel@zeiss.de
Customer No.
412284

Order confirmation 45/2020105648/08/09/2000
Delivery note 45/2030115091/08/09/2000

Consignee
CARL ZEISS, Inc. for
BOEHRINGER INGELHEIM
RSCH & DEVELOPMENT
175 BRIAR RIDGE ROAD
RIDGEFIELD CT 06877
USA

Your order NY/107-000001/PET from 05/26/2000

Customer PO: PE20408-00

Item.	PH	Article no.	Description	Value (USC)
		Quantity	Price (USD)	

000900 000000-1049-144 ConfoCor 2
Country of origin: Germany

Commodity code: 90119090

**REDACTED PRICING
INFORMATION**

Item includes subitems 001000 to 081002

001000 453067-0000-000 Transmitted-light channel with motorized switching mirror
1 PC

- 2 -

Vorsitzender des Aufsichtsrates:
Dr. Peter Grassmann

Geschäftsführung:
Dr. Franz-F. von Falkenhausen, Sprecher
Dr. Manfred Fritsch
Norbert Scheuch

Carl Zeiss Jena GmbH
Zeiss Gruppe

Hausadresse/Lieferanschrift

Carl Zeiss Jena GmbH
Carl-Zeiss-Promenade 10
07745 Jena
Bundesrepublik Deutschland

Amtsgericht Gera HRB 1296
UST-ID. Nr. DE 811 120 323

Banken:
Deutsche Bank Jena
Konto 397773300 (BLZ 820 700 00)

Hypo Vereinsbank Jena
Konto 4146999 (BLZ 830 200 87)
Commerzbank Jena
Konto 258182500 (BLZ 820 400 00)
Dresdner Bank Jena
Konto 348010000 (BLZ 820 800 00)
S.W.I.F.T.-address: DRES DE FF 825



Invoice 45 / 2040118607 / 08/10/2000

- 2 -

Item.	PH	Article no. Quantity	Description Price (USD)	Value (USD)
002000		453031-0000-000 1 PC	Large LSM 510 system table	REDACTED PRICING INFORMATION
004000		451331-0000-000 Serialno.:(610557) 1 PC	"Axiovert" 100 M SP LSM 5 microscope stand	
005000		451321-0000-000 1 PC	Binocular photo tube with sliding prism 45°/20	
006000		479321-0000-000 1 PC	Dust cover UMSP/LSM	
007000		447217-0000-000 1 PC	HAL Lamp Housing	
008000		457411-9050-000 1 PC	Extension cable for HAL 12V 100W	
009000		380079-9540-000 4 PC	Halogen lamp 12V 100W	
010000		458417-0000-000 1 PC	Power supply 12V DC 100W stabilized	
011000		451334-0000-000 1 PC	Illuminator carrier for "Axiovert" LSM 5	
012000		457411-9019-000 1 PC	Remote cable CSM lamp	
013000		451333-0000-000 1 PC	Reflector slider LSM 5 "Axiovert"	
014000		451383-0000-000 1 PC	Epi-fluorescence equipment FL	
015000		488001-0000-000 1 PC	Filter set 01 shift free	



Invoice 45 / 2040118607 / 08/10/2000

- 3 -

Item.	PH	Article no. Quantity	Description Price (USD)	Value (USD)
016000		488010-0000-000 1 PC	Filter set 10 shift free	REDACTED PRICING INFORMATION
017000		488015-0000-000 1 PC	Filter set 15 shift free	
018000		447220-0000-000 1 PC	Lamp housing HBO 50 with socket	
019000		447270-0000-000 1 PC	Lamp collector HBO 50/SF 25	
020000		381619-0000-000 2 PC	HBO 50 super-pressure mercury lamp	
021000		444232-9902-000 2 PC	Eyeplece E-PL 10x/20 Br.foc.	
022000		444801-0000-000 2 PC	Eyeplece eyecup	
023000		440330-0000-000 1 PC	Obiective "Plan-Neofluar" 10x/0.30	
024000		440542-0000-000 1 PC	Objective "Plan-Neofluar" 25x/0.80 Imm. corr. DIC	
025000		000000-1022-818 1 PC	Objective "Plan-Neofluar" 40x/1.30 Oil	
026000		440762-9902-000 1 PC	Objective "Plan-Apochromat" 63x/1.40 Oil DIC	
027000		440782-0000-000 1 PC	Objective "Plan-Apochromat" 100x/1.40 Oil DIC	
028000		451359-0000-000 1 PC	LD Condenser 0.55 Ph 1, Ph 2, Ph 3, DIC, DIC	



Invoice 45 / 2040118607 / 08/10/2000

- 4 -

Item.	PH Article no. Quantity	Description Price (USD)	Value (USD)
029000	440052-0000-000 1 PC	Objective "C-Apochromat" 40x/1,20 W corr.	REDACTED PRICING INFORMATION
030000	000000-1017-917 1 PC	Scanning stage DC 100x90	
031000	457428-0000-000 1 PC	Motor control MCU 28	
032000	457411-9011-000 1 PC	CAN-BUS cable 2.5 m	
033000	457433-0000-000 1 PC	2-axes control panel	
034000	000000-1030-764 1 PC	CD-writer extern YAMAHA CRW 4260tx (0)	
035000	000000-1075-094 1 PC	LSM 510 software updates for one year	
036000	000000-1066-725 Serialno.: (YBHE249268) 1 PC	Host computer for LSM 510 (O)	
037000	000000-1060-089 Serialno.: (YECN002443, YECN002444) 2 PC	Monitor SIEMENS MCM 21T2 21" (50cm) Trinitron (D)	
038000	000000-1064-939 1 PC	ECU - LSM 5 with scanner drive	
039000	000000-1018-215 1 PC	VIS scan module	
040000	000000-1023-896 1 PC	Channel 3	
041000	000000-1018-382 1 PC	Laser module VIS	



Invoice 45 / 2040118607 / 08/10/2000

- 5 -

Item.	PH Article no. Quantity	Description Price (USD)	Value (USD)
042000	000000-1074-135 1 PC	LSM 510 Basis Software Release 2.5 (1 CD)	REDACTED PRICING INFORMATION
043000	000000-1026-994 1 PC	Ar-laser 458 ,488, 514nm, 25mW with adaptation (integrated)	
044000	000000-1069-255 1 PC	HeNe-laser, 543 nm, 1 mW (integrated)	
045000	000000-1018-217 1 PC	HeNe laser, 633nm, 5mW (red) with adaptation (integrated)	
046000	000000-1018-221 1 PC	VIS AOTF (6 cannels)	
047000	447900-0000-000 1 PC	Neutral splitter 80/20	
048000	447905-0000-000 1 PC	Beam splitter UV, 488, 543, 633	
049000	000000-1016-466 1 PC	Primary color divider 514/633	
050000	000000-1016-464 1 PC	Primary color divider 458/543	
051000	447915-0000-000 1 PC	Beam splitter 488, 543	
052000	447922-0000-000 1 PC	Primary color divider 458	
053000	447923-0000-000 1 PC	Primary color divider 488	
054000	453001-4023-000 3 PC	Mirror	



Invoice 45 / 2040118607 / 08/10/2000

- 6 -

Item.	PH	Article no. Quantity	Description Price (USD)	Value (USD)
055000		447932-0000-000 2 PC	Secondary color divider 545	REDACTED PRICING INFORMATION
056000		447933-0000-000 1 PC	Secondary color divider 570	
057000		447936-0000-000 1 PC	Secondary color divider NFT 635 VIS	
058000		453001-4021-011 3 PC	Compensations plate	
059000		447942-0000-000 2 PC	Long bandpass filter LP 475, d=10	
060000		447943-0000-000 2 PC	Long bandpass filter 505, d=10	
061000		447944-0000-000 2 PC	Long bandpass filter LP 530, d=10	
062000		447945-0000-000 2 PC	Long bandpass filter LP 560, d=10	
063000		447946-0000-000 2 PC	Long bandpass filter LP 585, d=10	
064000		000000-1055-597 1 PC	Primary color divider HFT 458/514 for LSM 510	
065000		447949-0000-000 1 PC	Long bandpass filter LP 650, d=10	
066000		000000-1027-056 1 PC	Bandpass filter BP 475-525, d=10	
067000		447953-0000-000 1 PC	Bandpass filter BP 505-530, d=10	



Invoice 45 / 2040118607 / 08/10/2000

- 7 -

Item.	PH	Article no. Quantity	Description Price (USD)	Value (USD)
068000		447954-0000-000 1 PC	Bandpass filter BP 505-550, d=10	REDACTED PRICING INFORMATION
069000		000000-1016-482 1 PC	Bandpass filter BP 530-600	
070000		447955-0000-000 1 PC	Bandpass filter BP 560-615, d=10	
071000		447957-0000-000 1 PC	Bandpass filter BP 585-615, d=10	
072000		000000-1020-723 1 PC	Secondary color divider 514	
073000		457411-9140-000 1 PC	Cable set for LSM 510	
074000		000000-1048-919 1 PC	Kit for integration of second LSM port	
075000		000000-1082-283 1 PC	Universal mounting frame KN	
076000		000000-1048-920 1 PC	Kit for integration of DC scanning stage	
077000		000000-1020-688 1 PC	Retrofitting kit for beam switching	
078000		000000-1048-913 1 PC	ConfoCor 2 retrofitting kit for ECU-LSM 5	
079000		000000-1018-128 1 PC	Matrox Meteor2 Frame Grabber (D)	
080000		000000-1048-925 1 PC	ConfoCor 2 software upgrade for LSM 510 Release 2.5	



Invoice 45 / 2040118607 / 08/10/2000

- 8 -

Item.	PH	Article no. Quantity	Description Price (USD)	Value (USD)
-------	----	-------------------------	----------------------------	-------------

081000		000000-1048-916 Serialno.:(1102000123) 1 PC	ConfoCor 2 detection head, dual-channel VIS
--------	--	---	---

**REDACTED PRICING
INFORMATION**

081001		453025-8023-000 1 PC	Insert for power supply 120V (for USA/Canada) (O)
--------	--	-------------------------	---

081002		453001-4021-052 2 PC	Neutral splitter 50/50 IR
--------	--	-------------------------	---------------------------

Sum total of items

Total

FCA Frankfurt / Main



Invoice 45 / 2040118607 / 08/10/2000

- 9 -

Terms of payment:

Payment in full by the 25th of the month following delivery (invoice date), plus 60 days.

Terms of delivery:

FCA Frankfurt / Main

Dispatch route:

Standard terms

Shipping Marks:

CARL ZEISS, INC.
FOR BOEHRINGER INGELHEIM
RSCH & DEVELOPMENT
NY/107-000001/PET
THORNWOOD NY
USA
1/4 - 4/4

Packing:

4 colli total

collo	gross/net weight	size	cbm
1/4	277,00/180,00 kg	185x83x118	1,812
2/4	156,00/100,00 kg	160x93x 96	1,428
3/4	87,00/ 72,00 kg	121x81x 82	0,804
4/4	75,00/ 65,00 kg	95x71x117	0,789

total: 595,00/417,00 kg 4,833

We hereby declare that the wooden packing material are totally free from bark and apparently free from live plant pests.